QATAR UNIVERSITY

COLLEGE OF ENGINEERING

EXTERNALLY BONDED AND NEAR-SURFACE MOUNTED FRP STRIPS FOR SHEAR STRENGTHENING OF RC DEEP BEAMS

BY

MOHAMED AMIN BABIKER IBRAHIM

A Thesis Submitted to

the Faculty of the College of Engineering

in Partial Fulfillment of the Requirements for the Degree of

Master of Science in Civil Engineering

June 2019

COMMITTEE PAGE

The members of the Committee approve the Thesis of Mohamed Amin Ibrahim defended on 16/04/2019.

Prof. Usama Ebead
Thesis Supervisor

Dr. Wael Alnahhal
Committee Member

Dr. Mahmoud Taha
Committee Member

Dr. Mohammed Hussein
Committee Member

Approved:

Abdel Magid Hamouda, Dean, College of Engineering

ABSTRACT

IBRAHIM, MOHAMED, A., Masters: June : 2019,

Masters of Science in Civil Engineering

Title: Externally Bonded and Near-Surface Mounted FRP Strips for Shear Strengthening of RC Deep Beams

Supervisor of Thesis : Usama, A, Ebead.

This thesis presents an experimental study on the efficacy of fiber reinforced polymer (FRP) strips using externally bonded (EB) and near surface mounted (NSM) techniques for the shear strengthening of reinforced concrete (RC) rectangular deep beams. The experimental program included construction and testing of nineteen medium-scaled RC rectangular deep beams. Five beams were kept unstrengthened to act as references, while seven beams were strengthened using the EB technique, and the remaining seven beams were strengthened using the NSM technique. All beams have been tested under three-point loading with a displacement rate of 0.25 mm/min. A typical critical shear span to effective depth ratio (a/d =1.6) was fixed for all beams. The interaction between the shear stirrups and the strengthening systems has been investigated. The test variables included the FRP configurations (two, three, and four EB/NSM-FRP), steel stirrups at the CSS configurations (two, three, and nil), and the relation between steel stirrups and the strengthening system at the CSS (aligned and unaligned). The test results revealed that both EB and NSM techniques could be used to enhance the shear capacity and deformational characteristics of RC rectangular deep beams. The NSM technique has shown better performance with an average increase in the ultimate load capacity of 41.4%, while that was 10.1% for the EB technique.

DEDICATION

“To my grandparents, parents, and lovely brother.”

ACKNOWLEDGMENTS

First and foremost, I would like to thank Almighty Allah for his endless grants, blessings, and mercy. I am thankful to Allah for endowing myself with health, patience, and knowledge to undertake this research project and to complete it successfully.

Next, I would like to express my particular gratitude to my supervisor, Prof. Usama Ebead, for his consistent support, guidance, and supervision. I am proud of being one of his students since 2015 during my bachelor and master studies at Qatar University. Prof. Ebead was always trying to prepare me for the future by enriching my knowledge, research skills and directing me towards the professionalism. With his gentle care and constant guidance, I could be able to accomplish this thesis.

Furthermore, I would also like to thank the following people for their support. Without their kind assistance, this achievement would never be possible. I would also like to thank Eng. Siju Joseph, Lab Technician, for helping me to carry out the experimental work. Also, I would like to thank my research team individuals for their valuable support. Moreover, I would like to thank all my friends, who were always encouraging me to complete this project.

Finally, my deepest gratitude goes to my grandparents, parents and lovely brother for their continuous love, prayers, and great efforts in meeting all my needs to accomplish this project effectively and successfully.

TABLE OF CONTENTS

LIST OF TABLES

LIST OF FIGURES

NOTATION AND SYMBOLS

C	Carbon
CFRP	Carbon FRP
CSS	Critical shear span
CW	Crack width
EB	Externally bonded
FRP	Fiber reinforced polymer
G	Glass
GFRP	Glass FRP
LVDT	Linear variable displacement transducer
NSM	Near-surface mounted
RC	Reinforced concrete
E_s	Elastic modulus of steel
P_u	Ultimate load carrying capacity
δ_u	Deflection at the ultimate load
$\varepsilon_{c,u}$	Compressive strain developed in concrete at the ultimate load
$\varepsilon_{l,u}$	Strain developed in the flexural rebars at the ultimate load
$\varepsilon_{v,u}$	Strain developed in shear steel stirrups at the ultimate load
Ψ	Energy absorption
V_n	Nominal shear strength
V_c	Contribution of concrete in the shear strength

V_s	Contribution of steel stirrups in the shear strength
V_f	Contribution of FRP strips in the shear strength
ψ_f	Reduction factor for using FRP in both sides of the beams
L	Clear span between the supports
L_{cr}	Critical shear span length
A_{sv}	Area of steel stirrups
$f_{y_{sv}}$	Yield strength of steel stirrups
d	Effective depth
s	Stirrups spacing
A_{f_v}	Area of FRP to resist the shear forces
f_{f_e}	Total effective FRP stress
d_{f_v}	Effective depth of FRP
α	Angle of FRP inclination
w_f	Width of FRP strips
t_f	Thickness of FRP strips
ε_{f_e}	Effective strain of FRP strips
E_f	Modulus of elasticity of FRP strips
k_v	Reduction factor for the effective strain of FRP
ε_{f_u}	Ultimate FRP strain
f_c'	Compressive strength of concrete
P_u^{th}	Theoretical ultimate shear capacity

CHAPTER 1: INTRODUCTION

1.1 Hypothesis and Research Problems

Nowadays, the strengthening of reinforced concrete structures has become one of the most important practices in the construction industry. Strengthening and rehabilitation constitute an economic and environmentally viable alternative to demolition/reconstruction [1]. Deteriorated and deficient structures require effective strengthening/repair to ensure the safety of people using these structures.

Many factors cause deterioration of structures; e.g., corrosion of steel reinforcement bars, improper maintenance, unaccounted for service load augmentation, increase in the live load or change the original building purpose, errors on the design and/or construction process, and natural disasters. Recently, there have been numerous studies on different strengthening techniques and materials for deficient concrete structures, that aim at extending their lifetime span [2–6].

Some materials are effectively used for structure strengthening, such as steel plates [7,8], ferrocement [9,10], fiber reinforced polymer (FRP) composites, and fabric reinforced cementitious matrix (FRCM) [11–16]. FRP composites are commonly used for the strengthening of different reinforced concrete elements [17–22]. Existed literature showed the effective use of FRP as a strengthening material in a variety of structural applications, such as column confinement [23–25], flexure strengthening of RC slab [26–31], flexure strengthening of RC beams [32,33] and shear strengthening of RC beams [18,34–36].

There are some special types of structural elements such as deep beams, which are differentiated from the slender beams by their relatively small span to depth ratio (l/d). The deep beam is involved in many applications; namely, offshore structures, wall footing, foundation pile caps, floor diaphragms, shear walls, and nuclear power plant structures [18,37]. State of the art review on the available literature shows a shortage of the research contributions developed to study the shear strengthening techniques for RC rectangular deep beams, particularly using the NSM technique.

In light of the after-mentioned gap, the present research work introduces a comprehensive study of using the NSM-FRP and EB-FRP to shear-strengthen the rectangular RC deep beams and the interaction between the steel stirrups and FRP strips.

1.2 Aims and Objectives of the Study

This research generally aimed to assess the feasibility of utilizing the NSM-FRP and EB-FRP for the shear strengthening of rectangular RC deep beams. The main objectives of this research are listed as follows:

- To investigate the efficacy of the NSM-FRP and EB-FRP techniques to enhance the load capacity of the rectangular RC deep beams that are shear-deficient.
- To study the effectiveness of various configurations of FRP on the load capacity and deformational characteristics of the specimens.
- To investigate the interaction between the FRP and the steel stirrups at the CSS.
- To investigate the failure mechanisms of the deep beams strengthened using the NSM and EB techniques.

1.3 Methodology

This research includes three test parameters; namely, (a) FRP configurations: two, three, and four FRP strips, (b) strengthening techniques: NSM-FRP and EB-FRP, and (c) The FRP/stirrups interaction: aligned verses unaligned configurations. For this purpose, a series of nineteen (19) medium-scaled RC deep beams (shear span to effective depth ratio a/d=1.6) are fabricated with the dimensions 400 mm × 150 mm × 2200 mm (height × width × length). The beams were designed with five (5) different steel stirrups configurations to study the FRP/stirrups interaction. Specimens are used as follows: seven specimens are strengthened using NSM-FRP technique, seven specimens are strengthened using EB-FRP technique, and five specimens are kept non-strengthened as references. The beams are tested under 3-point monotonic loading at a constant displacement rate of 0.25 mm/min. The experimental results were mainly investigated in terms of the load carrying capacity, deformational characteristics, failure modes, and strain results.

1.4 Structure of the Thesis

Chapter 2: Literature Review and Background– this chapter presents a general background, and up to date literature review in the shear strengthening of RC beams.

Chapter 3: Experimental Program – this chapter includes material properties, test matrix, specimen's description, and preparation, strengthening procedures, test setup, and instrumentations.

Chapter 4: Results and Discussion – this chapter includes a discussion for the experimental results and the influence of different test parameters in the load carrying capacity, deflection, crack width, failure modes, and strains.

Chapter 5: Summary and Conclusions– this chapter summarizes the most important findings that could be concluded from the observed test results.

CHAPTER 2: BACKGROUND AND LITERATURE REVIEW

This chapter starts with a background and introduction of the importance of the strengthening process for RC structures. Then, up to date literature review is provided for the known strengthening techniques and materials. Eventually, a special emphasis is placed on the related previous research work.

2.1 Introduction and Background

Concrete is a material that consists mainly of cement, fine and coarse aggregates, and water. It is the most versatile construction material, especially when it is reinforced with steel rebars. However, unfortunately, the concrete structures become deficient and/or structurally deteriorated due to several factors. The primary cause for structural deterioration is the effects of the corrosion process of reinforcement steel rebar. Another factor for structural deterioration is the augmentation, that is unaccounted when determining the service load. Errors in design and/or construction can also be considered among the critical causes of structural deterioration. Also, the structure may also be damaged due to severe natural disasters such as hurricanes, earthquake evens and fire. In addition, the structures can be affected by riots, terrorism, and wars.

Deficient and deteriorated structures require the decision maker to effectively remedy their harmful effects to ensure the safety of people using these structures. In order to address these effects, there are two options, i.e., demolition and reconstruction or structural rehabilitation/strengthening. Structural strengthening/rehabilitation can be much-preferred alternative economically and environmentally as concluded by the assessment study performed by Alba-Rodríguez et al. [1]. The same conclusion was drawn by other authors [38,39].

Also, there are some of the structures, that have their historical and cultural values, which make them unwanted for demolition. Consequently, nowadays, strengthening has become one of the most attractive topics for research. Actually, there are numerous strengthening techniques and materials, that scholars have extensively studied. Generally, the structural strengthening process is mainly utilized to enhance the capacity of the structural elements to carry more loads than designed, to recover the original functionality of the deficient structural elements and/or to reduce the deflection caused by overloading.

RC beams are structural elements transferring the loads from floor slabs to columns. The RC beams commonly fail due to flexure or shear forces. The shear failure mode occurs more frequent with short and heavy loaded beams owing to the sliding and tearing of the molecules of the beams' materials. It usually happens at 45-degree in the compression zone between the applied load and supports as shown in Figure 1. Therefore, beams are reinforced with steel stirrups to resist the shear stresses as well as reinforced with longitudinal steel rebars to withstand the flexure stresses. Shear strengthening of the RC beams is just adding shear reinforcement externally to support the internal shear reinforcement (stirrups).

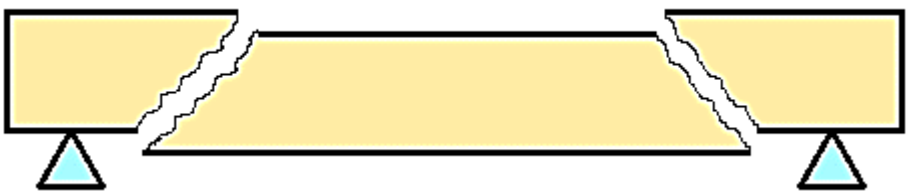

Figure 1: Shear failure for RC beams.

2.2 Traditional Strengthening Systems

Traditional strengthening techniques use steel and concrete for structural strengthening. The most common conventional methods that can be used for the shear strengthening include but not limited to reinforced concrete jacketing, internal and external post-tensioning, and span shortening.

Reinforced concrete jacketing is performed by enlarging the concrete section by installing additional steel bars after removing the concrete cover. This technique is most commonly used for columns. It significantly increases the columns' shear and axial strength, [40]. The same concept of expanding the cross-section is applied to other types of structural members such as beams, walls, and slabs to increase their capacities of caring more shear forces. Also, it can be used for other types of structural strengthening applications such as flexural, torsion, and axial forces. Figure 2 shows an example of cross section enlarging of columns using the RC jacketing.

Figure 2: RC columns were jacketing [41].

External/internal post-tensioning strengthening has a successful history since the 90s. The external post-tensioning can relieve stresses, reduce the excess of deflections, improve the fatigue details, and eventually enhance the load carrying capacity of the structural element. The external and internal post tension strengthening techniques are illustrated in Figures 3 and 4, respectively [42].

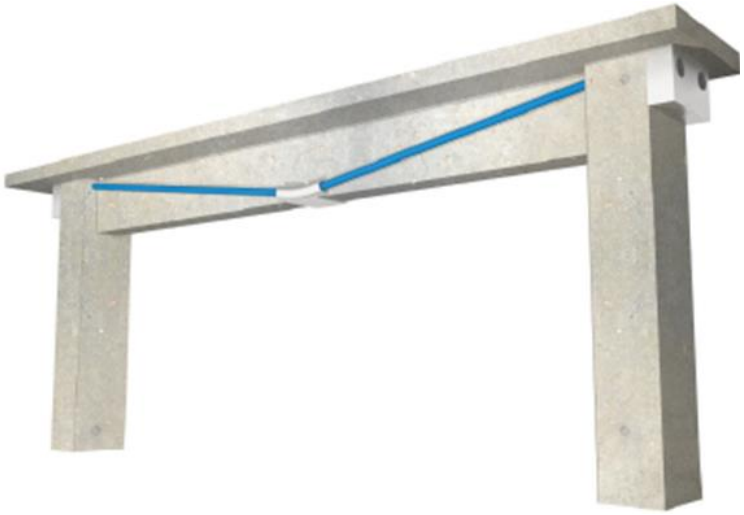

Figure 3: External post-tensioning of beam [43].

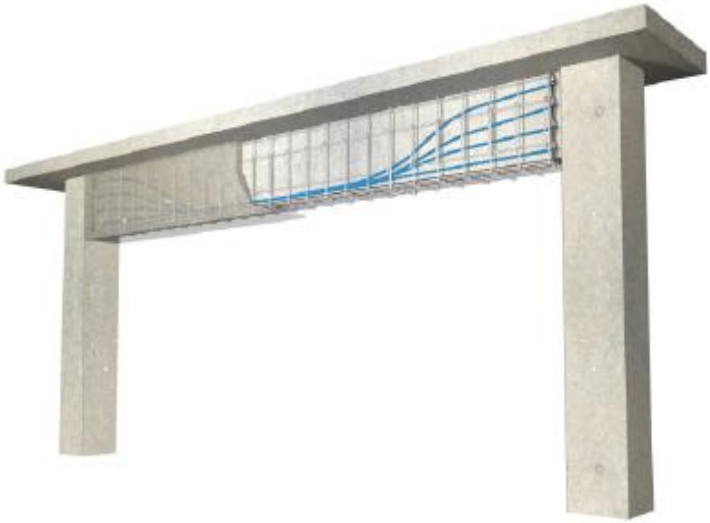

Figure 4: Internal post-tensioning of beam [43].

Span shortening technique contributes to reducing the span length of the applied load by adding additional supports at the critical zones [44]. The extra support can be structural steel or reinforced concrete member. The connection between the existing member and the newly added member can be made by adhesive anchors, bolts, cementitious mortar, or any other binding materials. Reducing the span of the structural member leads to decrease in the applied stresses on the structural members. This technique can be used to enhance the shear capacity of the beams and slabs. Figure 5 shows the span shortening system by adding a steel column to strengthen a parking floor slab.

Figure 5*:* Strengthening of parking garage slab by span shortening [44].

Although these traditional techniques have shown a significant contribution to structural strengthening for many years, they have some drawbacks. Firstly, the structures would be subjected to extra load due to the additional weights of the added concrete and steel. This may negatively affect the neighboring structural elements. Also, these techniques require more time, effort, and cost for the installation of the additional strengthening materials. Moreover, the materials used for traditional strengthening are susceptible to corrosion, leading to further deterioration. In order to overcome these drawbacks, scholars have studied numerous strengthening materials and systems to replace traditional strengthening techniques.

2.3 Fiber Reinforced Polymer (FRP) Composites

2.3.1 Introduction for FRP Composites

Fiber reinforcement polymer (FRP) composites are commonly used for the strengthening of different reinforced concrete structural elements [17–22]. Typically, they are classified into; glass FRP (GFRP), carbon FRP (CFRP), aramid FRP (AFRP), and basalt FRP (BFRP). The most commonly used materials of FRP for strengthening are the CFRP and GFRP due to their high tensile and ductility properties, respectively. However, FRP can also be made by combining varied materials to generate a hybrid FRP composite that gather the advantages of these materials. Recently, FRP composites have been increasingly popular in the construction industry owing to their favorable properties. First of all, FRP can be easily pultruded as required in the field. The strengthening process can be more efficient, rapid, and effective with the use of FRP.

The FRP composites are commonly used in the form of plates, strips, sheets, rods, and laminates. The major strengthening techniques of using FRP include the externally bonded (EB) system, and the near surface mounted (NSM) system.

2.3.2 Externally Bonded Technique

EB system is the most commonly used strengthening technique considering its ease of application. Generally, it has been used to strengthen the structural elements for flexure, axial, torsion, and shear. There are several shear applications that have been studied using the EB technique. The EB system typically consists of applying the FRP composite to the concrete cover of the deficient structural member using epoxy resin, adhesive anchors, cementitious mortar, or mechanical fasteners. Sometimes the system can be used by combining two methods; resin/mechanical fasteners system, or adhesive anchors/cementitious mortar system.

Nevertheless, there are some drawbacks of EB technique such as premature debonding of FRP composite from the concrete substrate, low fire-resistance causing bond deterioration at elevated temperatures due to full exposure, and the inability to be applied on the wet surfaces. In order to overcome these issues, the NSM-FRP strengthening technique is introduced.

2.3.3 Near Surface Mounted Technique

The NSM strengthening technique has gained scholars' attention as a preferable alternative to the EB system. Numerous research contributions have successfully proven its feasibility to effectively enhance the shear load carrying capacity and the deformation characteristics of the strengthened structural members. The NSM strengthening system is considered recent strengthening technique compared to EB counterpart. Generally, the NSM system is composed of embeding additional reinforcement inside the concrete cover of the deficient structural member [45–47]. This technique has outperformed most of the other methods, due to its convenience to perform a significant enhancement on the structural member's capacity [48].

Moreover, this technique involves preserving the aesthetics of structural member to and adequately protects the strengthening material from exposing to the atmosphere's harmful factors. It has proven through several studies [48,49] that the NSM technique can be used to mitigate debonding between FRP and concrete. This mode of failure limits the strengthening material from using its full capacity. However, the debonding mode of failure seems to be the primary mode of failure in other strengthening techniques, e.g., EB-FRP.

2.3.4 Reinforced Concrete Deep Beams

RC beams are classified into two major types: slender and deep beams. Generally, deep beams are recognized by their relatively small span-to-depth ratio. According to ACI 318-11 code [50], a beam is classified as a deep beam if it has either: clear span (L) to overall depth (h) ration (L/h) is less than or equal to 4, or the region of concentrated loads within 2h away from the nearest support edge. In other words, beams with shear span (a) to an effective depth (d) ratio less than or equal to 2 are considered deep beams. The deep beam is involved in many useful applications; namely, offshore structures, wall footing, foundation pile caps, floor diaphragm, shear wall, and nuclear power plant structures [18,37]. The utilization of deep beams for connecting floors in the high-rise buildings for both residential and commercial purposes has substantially increased nowadays, due to its convenience and economic efficiency [51]. Admittedly, deep beams behave utterly different from slender beams due to the arch action of load transferring while bending. The traditional assumptions of designing the slender beams, particularly, the assumption of the plane cross section before bending remains plane after bending, are not applied with the deep beams [52].

Therefore, attention has to be paid while studying the behavior of the RC deep beams. Owing to the small span-to-depth ratio, the main design criteria of the RC deep beam is the shear strength. Consequently, deep beams will require typical strengthening for the shear capacity more than flexure [53]. Regards the shear strengthening for RC beams, it was found that the research available on the slender beams is considerably more than that for the deep beams.

2.3.5 Shear Strengthening of RC Slender Beams

Numerous studies have been conducted in the shear strengthening of RC slender beams. Rizzo and Lorenzis [17] have studied the feasibility of using the carbon FRP (CFRP) to enhance the shear load carrying capacity of the slender beams. The authors have studied the efficacy of NSM CFRP strips and round bars, as shown in Figure 6. For comparison purpose, one specimen was strengthened using EB laminates. Results concluded that using NSM-CFRP bars, NSM-CFRP strips, and EB-CFRP laminates increased the shear strength of the beams by 44%, 41%, and 16%, respectively, compared to the unstrengthened reference beam. Additionally, other researchers have found that the shear strength of RC slender beams could be enhanced in the range of 17% to 25% by CFRP bars which have been applied using the NSM technique [54].

(a) Rods (b) Strips

Figure 6: CFRP rods and strips [17].

Dias and Barros [55] also conducted a study on the efficiency of NSM-CFRP laminates to strengthen RC slender T-beams. The study included a comparison between the NSM and EB techniques. The authors concluded from the experimental results that the NSM technique was more effective than EB counterpart in terms of providing a higher strength gain. The average increase in the shear capacity when using the EB system was 47% of that when using the NSM counterpart.

Al-Mahmoud et al. [56], have also studied the efficacy of the NSM CFRP rods to increase the shear capacity of the slender beams. They have inserted the CFRP rods to the concrete cover of the beam as shown in Figure 7. The authors compared using epoxy resin and cementitious mortar as a filling material. Results proved that both resin and mortar were sufficient to play the filling material role in the NSM strengthening techniques. However, the increase in the shear capacity for the beam specimens with mortar was higher than that with epoxy resin. Overall, the average increase in the capacity of the beams was around 37% compared to the reference beam specimen.

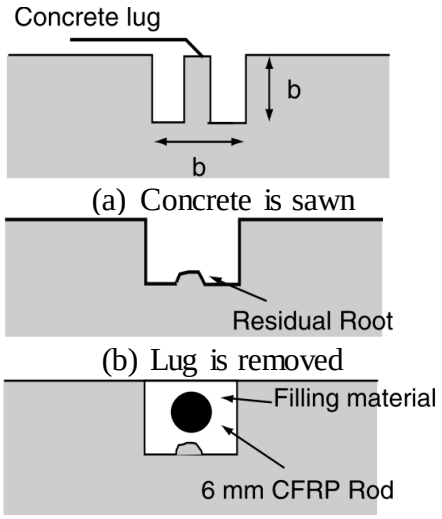

Figure 7: Installation of NSM- CFRP rods [56].

Lorenzis and Nanni [57], conducted a research study on using the NSM-CFRP rods to strengthen the shear capacity of RC slender T-beams. The research examined the effect of using inclined (45-degree) as well as straight FRP rods, and the usage of anchors at the flange of the beam. The authors studied beam specimens with and without steel stirrups to determine the contribution of the strengthening technique. Results showed an overall significant increase in the shear capacity using the NSM-FRP strengthening technique. However, the increase percentage varied with the various configurations. For example, the beam reinforced with steel stirrups showed an increase of 35%, while that increase was reported up to 100% for the strengthened specimens without steel stirrups. The authors have also noticed that replacing the straight FRP rods by 45-degree rods enhanced the shear capacity by an average of 42%, based on the used amount of FRP. Finally, they concluded that the most efficient way to increase the shear capacity of RC T-beam is by using the NSM-FRP rods anchored to the flange as the usage of the anchors at the flange recorded an increase of 45% with respect to an identical strengthened beam without anchors.

This conclusion has also been confirmed by Rahal, and Rumaih [58] who have conducted research on the usage of NSM steel and NSM CFRP rods to increase the shear strength of RC T-beams. They have reported an increase in the shear capacity over the control beam of 47% using CFRP rod without anchors, while that ratio was 69% with the existence of anchors at the flange of the beam. Regarding the steel rods, results showed that using them anchored to the flange provide 18% more in the shear capacity.

Chaallal et al. [59], experimentally tested six full-scale RC T- beams to conduct a comparison between different techniques including NSM and EB to enhance the shear capacity of the beams using CFRP. The EB technique has been applied by covering both sides of the beam with the CFRP sheets in U-shape, as shown in Figure 8a. For the NSM. The authors inserted the CFRP rods to inside grooves of 15 mm in the concrete cover of the beam, as shown in Figure 8b. Eventually, the results showed that the shear capacity of the beam increased by an average of 23% and 31% using the EB and NSM techniques, respectively. They have also reported that beams strengthened with EB failed by debonding of the FRP sheets and beams strengthened with NSM failed by concrete cover separation at steel stirrups location.

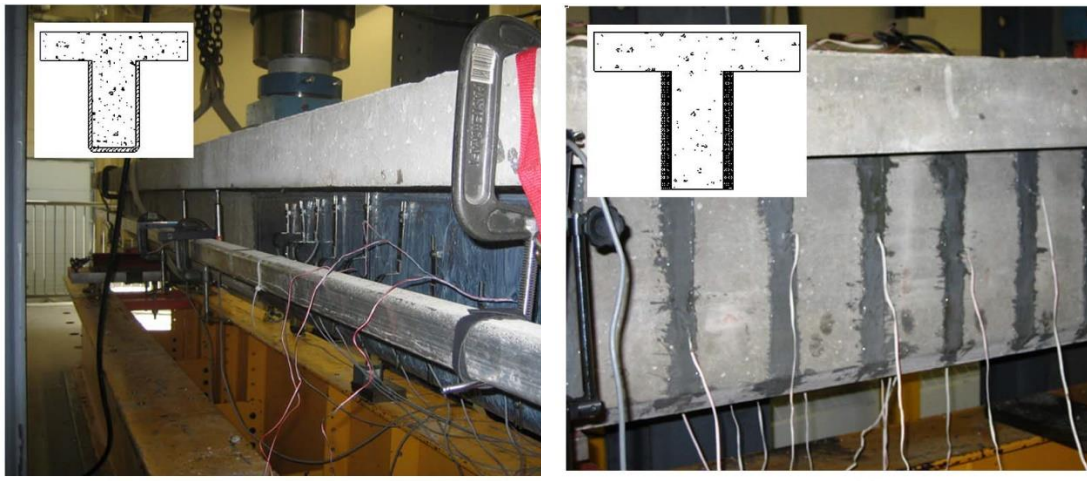

(a) (b)

Figure 8: Strengthening techniques used by Chaallal et al. [59] (a) U-wrapping EB-CFRP; (b) NSM-CFRP rods.

The interaction between the steel stirrups and the FRP strips for shear strengthened RC slender beams has been studied by Ebead and Saeed [22]. The study included twelve RC slender beam specimens; six specimens were fabricated with steel stirrups at the critical shear span, and six specimens were fabricated without steel

stirrups. From the experimental results, they noticed that the more increase in the load carrying capacity due to shear strengthening, the less effect of the steel stirrups in the shear resistance at the critical shear span, where the FRP is applied.

The same conclusion was drawn by Grande et al. [60], who tested fifteen RC slender beams to investigate the interaction of the transverse shear stirrups in the shear span to the FRP strengthening performance. They found that the contribution of the FRP to resist the shear forces reduces as the internal shear stirrups increases.

2.3.6 Shear Strengthening of RC Deep Beams

A scant number of studies available on the literature for the shear strengthening of the RC rectangular deep beams. Islam et al. [61], have studied the feasibility of using the FRP externally bonded to enhance the shear capacity of RC deep beams. The authors have applied the FRP to the sides of the beam specimens at an inclined and vertical orientation. Also, they used a full U-wrapping technique to cover both sides of the beam, as shown in Figure 9. Results showed an average increase of 40% in the shear capacity referenced to the non-strengthened beam [61].

Zhang et al. [62], have found anchored U-wrapped EB-CFRP significantly increases the shear capacity, the initial stiffness, and ductility of the RC deep beams. The authors have also concluded that the effectiveness of the anchors is related to the shear span to effective depth ratio (a/d) of the beam. There was an increase in the shear capacity of the deep beams with a/d = 1.9 or more, but there was no considerable effect of the anchors for the deep beams with a/d =1.25 or less.

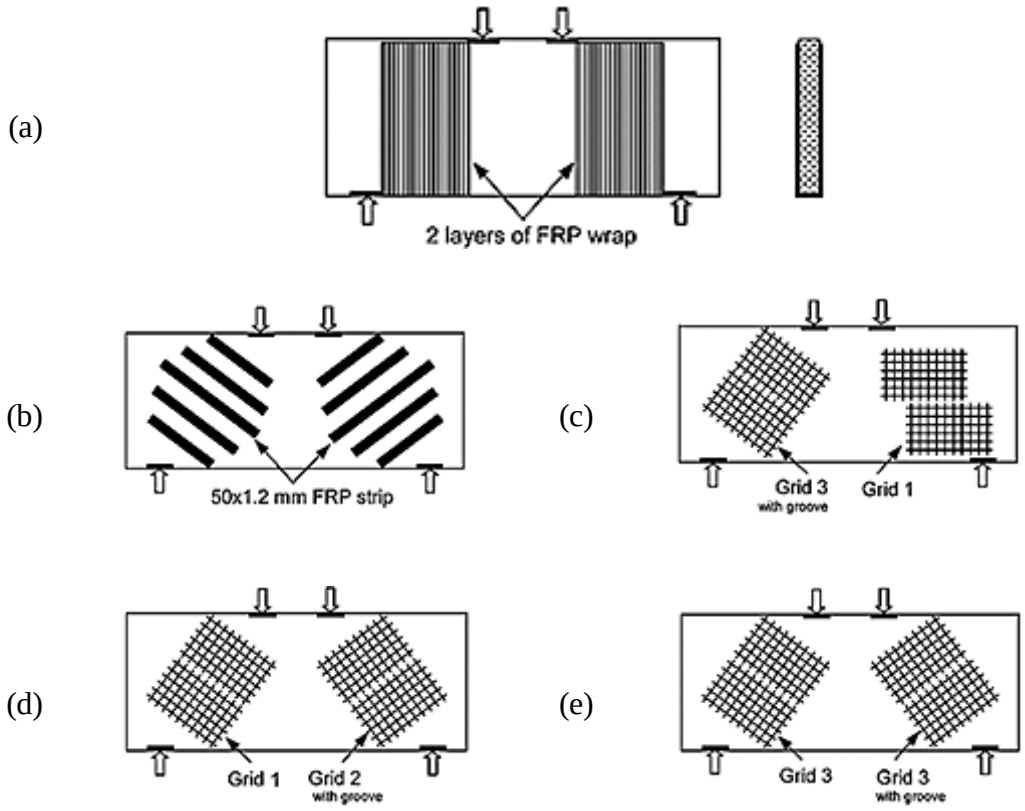

Figure 9: Arrangement of externally bonded FRP systems [61].

Almassri et al. [63], investigated the efficacy of using CFRP rods to repair corroded 28 years old RC deep beams with different (a/d) ratios. Generally, results showed an increase in the shear capacity of the beams ranged from 17% to 25 %.

Lee et al. [64], studied the performance of RC deep T-beams strengthened using EB-CFRP sheets. They included several test parameters such as the orientation of applying the sheets, the number of sheet layers, and the existence of anchors to the flange. The authors examined a total of 14 RC deep T-beams with a/d ratio = 1.22. They concluded that the governing mode of failure was shear compression failure owing to partial delamination of the FRP sheets. Overall, the shear carrying capacity of the strengthened deep beams was increased in the range from 15% to 66%. The shear capacity and the deformation characteristics of the deep beams have also been enhanced as shown in the load-displacement graph in

Figure *10* for the strengthened specimens.

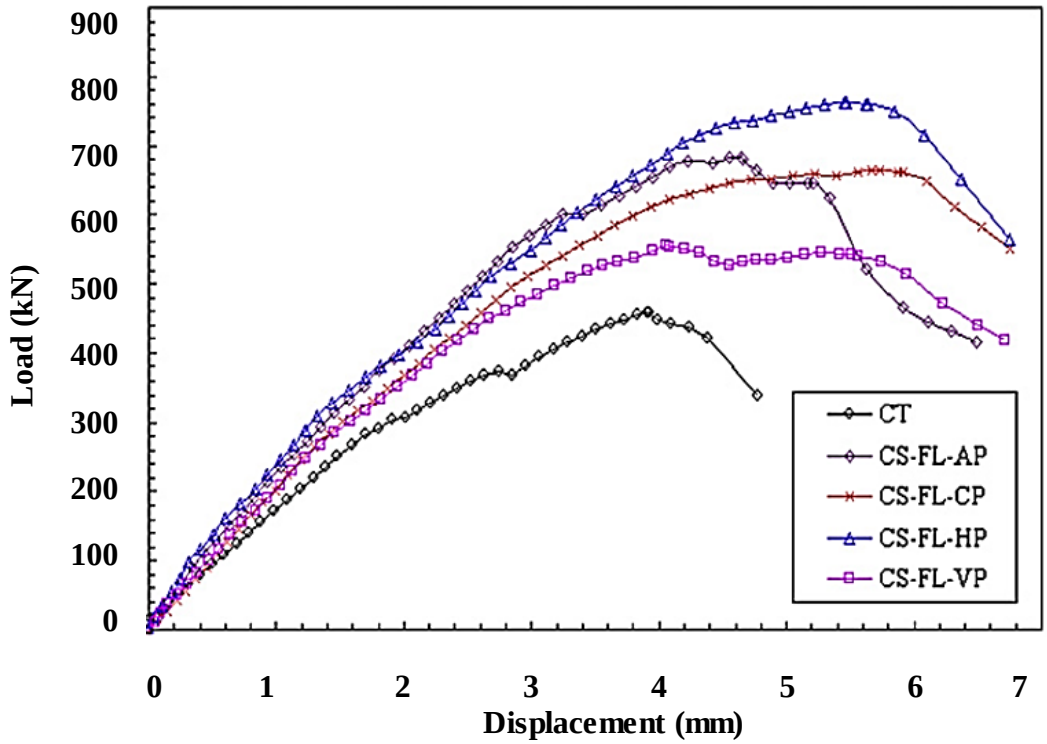

Figure 10: Load-displacement of Lee et al. [64] "CT" curve denotes to the control unstrengthened beam.

Bousselham and Chaallal [65], have conducted such an interesting study to compare the efficacy of using the CFRP externally bonded to enhance the shear capacity of RC slender and deep T-beams. They have tested the beam specimens in a 3-point loading condition that allowed each beam to be tested twice. Firstly, they have applied the load at a distance (a = 1.6d) from one side of the beam, while leaving the other side overhung and unstressed. This makes the beam to act as a deep beam. Next, they applied the load at the other side of the beam at a distance (a = 3d), while keeping the previously loaded side overhung. This makes the beam to act as a slender beam. As they have claimed, the sequence of loading beam specimen to serve as a deep beam then slender beam was not chosen arbitrarily because the specimens, as well as the test

setup, were designed accordingly. This testing program is illustrated in Figure 11.

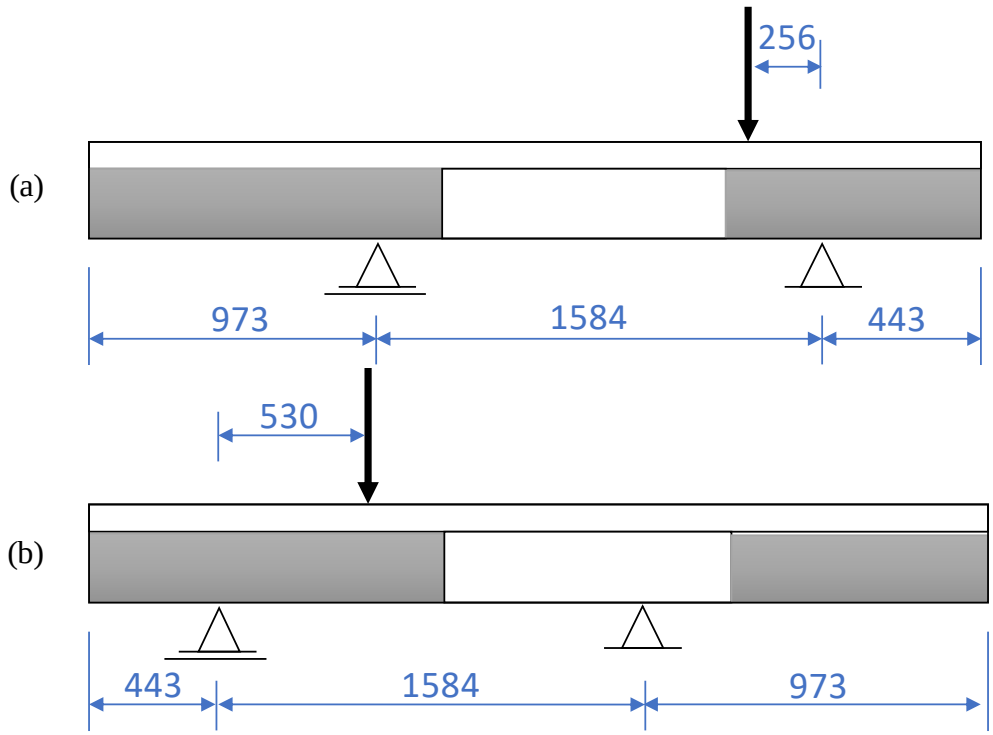

Figure 11: Test setup of Bousselham and Chaallal [65] study where (a) test on the deep beam, and (b) test on the slender beam. Dimensions in mm.

Ultimately, the results revealed an average increase of 10% and 43% in the shear capacity for the deep beams and slender beams, respectively, and concerning the reference beam. Scholars have also concluded that the existence of steel stirrups at the shear span have an effect of the FRP strengthening contribution for the slender beams; however, there was no a considerable effect of the steel stirrups on the deep beam. The strengthened slender beams have reached an average increase of 8% in the shear capacity with the existence of steel stirrups and 77% with the absence of steel stirrups. In contrast, the strengthened deep beams got an average increase in the shear capacity 10%, regardless of the steel stirrups.

2.3.7 Summary of the Related Literature Studies

To sum up, most of the studies showed an effective increase in the shear capacity by using either NSM or EB techniques. However, the NSM showed better performance over the EB technique. Generally, the strengthening of deep beam results in a lower ultimate load gain % than that for the slender beam. There is a limited number of research studies have been conducted in the shear strengthening RC deep beams, especially in the last five years. Although the proven success of the strengthening techniques to enhance the shear carrying capacity of the RC beams, there are several factors substantially affecting the efficiency of the strengthening materials and techniques. These factors can significantly vary the shear strengthening gain of the deficient structural elements.

The geometry of the specimens affects the shear capacity as well as the shear strengthening efficiency [52,53,66,67]. It is found that the shear span to effective depth ratio (a/d) has a significant effect on the FRP contribution to enhance the shear capacity of the beam. To illustrate, as the shear span to effective depth ratio (a/d) reduces, then so does the strengthening efficacy. This is attributed to the increase of the arch action of the beam whereby the loads are transferred [52].

As mentioned previously, the results of Bousselham and Chaallal [65], showed that the shear capacity was increased by an average of 77% for the slender beams with (a/d = 3) and only 10% for the deep beams with (a/d = 1.5). Also, Belal et al. [63] concluded that there was no marked effect of using NSM CFRP rods to strengthen corroded deep beams with (a/d) less than 2.

In addition to the (a/d) ratio, there are some other factors affecting in the shear strengthening performance, including the usage of mechanical anchorages with the U-wrapping EB technique, the depth of inserting the strengthening materials into the concrete cover with NSM technique, and the existence of steel stirrups along the shear span. Firstly, the usage of anchorages in U-wrapping externally bonded carbon FRP system, can significantly increase the FRP contribution to increasing the load carrying capacity, the initial stiffness, as well as the ductility of the RC deep beams as concluded by many researchers [57,62,64].

Moreover, the depth of grooves in the NSM strengthening technique is also a valuable factor as concluded by Barros and Dias [67]. Accurately, they reported that the effectiveness of the NSM shear strengthening technique for T-cross section deep beams is proportional to the depth of inserting the FRP laminates inside the cover of the beam's web [67]. The deeper the FRP plates are installed, the more effective is the NSM technique. However, the slits where the FRP plates are inserted are fundamentally limited by the concrete cover of the beam web, which is usually not exceeding 40 mm [67]. Finally, the existence of the steel stirrups in the shear span has found to decrease the shear strength gain the FRP, as concluded by several studies [65,68,69].

CHAPTER 3: EXPERIMENTAL PROGRAM

3.1 Material Properties

3.1.1 Concrete

A single batch of ready-mixed concrete has been used to cast all the specimens. Each one cubic meter of concrete comprised of 800 kg of fine aggregates, 1100 kg of course aggregates and 371 kg of cement. The water-to-cement ratio was fixed to be 0.44. Additionally, ten standard concrete cylinders (150 mm × 300 mm) were cast in order to evaluate the compressive and tensile strength of the concrete. Seven cylinders were tested for the compressive strength according to the ASTM C39/C39M [70] as shown in Figure 12, while three cylinders were tested for tensile strength using the splitting test according to the ASTM C496 / C496M [71]. The average 28 days the compressive and tensile strength was observed to be 40 ± 1.5 MPa and 2.93 ± 0.45 MPa, respectively.

(a) (b) (c)

Figure 12: Concrete cylinder specimen (a) before the test (b) during the test, and (c) after the test.

3.1.2 Steel Reinforcement

Overall, three sizes of steel rebars were used for all test beams specimens: 16, 8, and 6 mm diameter steel bars as shown in Figure 13. Four 16 mm diameter ribbed steel bars (double layers) were used as longitudinal tensile reinforcement, while two 8 mm diameter ribbed steel bars were used as compressive steel reinforcement. For the shear reinforcement (stirrups), 8 mm diameter ribbed steel bars with 100 mm center-to-center spacing were used along the whole beam except the critical shear span (CSS). For CSS, the number of stirrups depends on the specimen configurations; either no stirrups or 6 mm diameter steel bars with 200 mm or 135 mm center-to-center spacing.

The average yield stresses were observed through tensile test following the ASTM A370-17A [72] as shown in Figure 14. The results showed the average yield stress was 595 MPa for the 16 mm diameter bar, while that was 298 MPa and 234 MPa for the steel bars 8 mm and 6 mm, respectively. The other properties of steel bars are listed in Table 1.

Figure 13: Steel bars used in the test; namely, 16 mm, 8 mm, and 6 mm diameter bars.

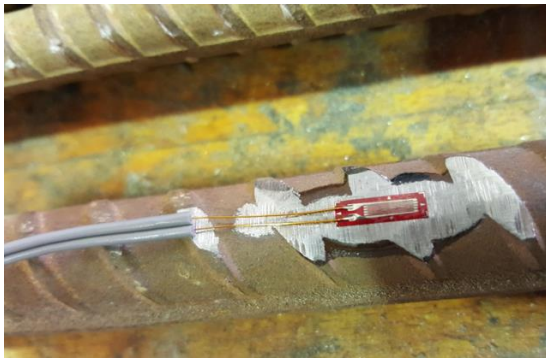

(a) Strain gauge insulation before the test

(b) Broken Specimen after tensile test

(c) Specimen during the tensile test

Figure 14: Tensile test for steel rebar.

Table 1:

Properties of the Steel Bars

Bar Diameter (mm)	Yield stress (MPa)	Yield strain ε_y (%)	Modulus of Elasticity (GPa)
6	234	0.115	204
8	298	0.144	207
16	595	0.266	224

3.1.3 Fiber Reinforcement Polymer (FRP)

SAFSTRIP® FRP was used for strengthening reinforcement. These FRP strips are composed of carbon tows sandwiched between two layers of glass fiber mats as depicted in Figure 15. The composite is bonded using high vinyl-ester resin. This combination of materials has increased the performance of the FRP strips as the carbon increases the stiffness, while glass increases the bearing capacity of the strip [73].

The dimensions of the FRP strip measured 100 mm in width 3.18 mm in thickness as depicted in Figure 15. The FRP was shipped in rolls of length 30.5 m as shown in Figure 16. However, this FRP was designed to be easily cut in the site using a carpenter standard cutting tool. The 3.18 mm thick FRP strips have been cut into strips of 25 mm wide and 400 mm long to be used in the NSM system. For the EB system, the FRP strips have been cut into 50 mm wide and 400 mm long with the same thickness 3.18 mm. The mechanical properties of the FRP strips are summarized in Table 2.

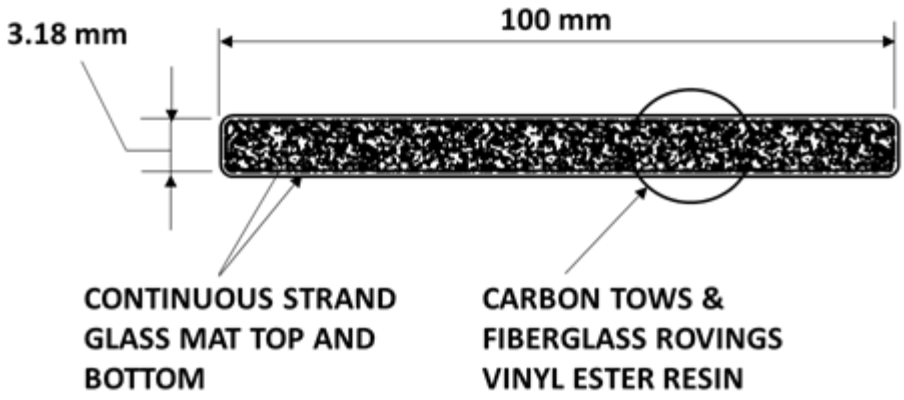

Figure 15: FRP strip cross-section [73].

Figure 16: FRP as delivered by the manufacturer.

Table 2:

Properties of Fiber Reinforced Polymer Strips as Reported by the manufacturer [73].

Property	Average Value (MPa)
Tensile Strength	852
Clamped Bearing Strength	351
Unclamped Bearing Strength	214
Open Hole Strength	652
Modulus of Elasticity	62190

3.1.5 Epoxy Resin

Sikadur® 30 LP epoxy adhesive resin was utilized in the installation of FRP strips inside the prepared grooves for NSM specimens. The same epoxy was used to bond the FRP strips to the beam concrete surface for EB specimens. This epoxy was delivered by the manufacturer as two components (A + B) as depicted in Figure 17. Typically, a mixture is made by mixing a ratio of (1:3) from (B: A). This epoxy is suitable to be used in the tropical and hot climates. Whereas, it is specially designed to perform effectively at hot temperatures (+25 °C to +55 °C). The mechanical properties of the epoxy are presented in Table 3 [74].

Figure 17: Epoxy as delivered by the manufacturer.

Table 3:

Properties of Epoxy as Reported by the manufacturer [74].

Properties	For Curing Temperature +25 ˚C	For Curing Temperature +55 ˚C
Tensile Strength (MPa)	17.5	28
Compressive Strength (MPa)	85	110
Modulus of Elasticity (MPa)	10000	10000

3.2 Test Specimens and Test Matrix

The experimental test matrix is summarized in Table 4. The test program involved nineteen (19) medium-scale RC rectangular beams. The beam dimensions are 2100 mm in length, 150 mm in width and 400 mm in depth. A constant concrete cover of 27 mm has been kept from all sides, leading an effective depth of 345 mm as shown in Figure 18. Five beam specimens were kept unstrengthened for references. The remaining fourteen (14) beams were strengthened for the shear using FRP. From the total strengthened fourteen (14) beams, seven (7) beams were strengthened using NSM technique and seven (7) beams were strengthened using EB technique as shown in Table 4.

All beams were 3-point monotonically loaded with a clear span of 1900 mm between the supports. The loading point was applied 550 mm from one support and 1350 mm from the other support as shown in Figure 18. This has allowed creating a critical shear span (a = 550 mm). Consequently, all the beams are considered deep beam as the shear span to effective depth ratio (a/d= 1.6) which is less than 2 as per ACI 381-11 code [50].

In order to achieve the goals of the research efficiently, the reinforcement of the beams has been designed to make the beam shear-deficient only at the critical shear span. Consequently, as indicated through preliminary calculations, the beams will tend to fail mostly on a compression shear mode at the critical shear span (CSS) only. Therefore, it is a representation of a real case of RC beams that are deficient in shear strength.

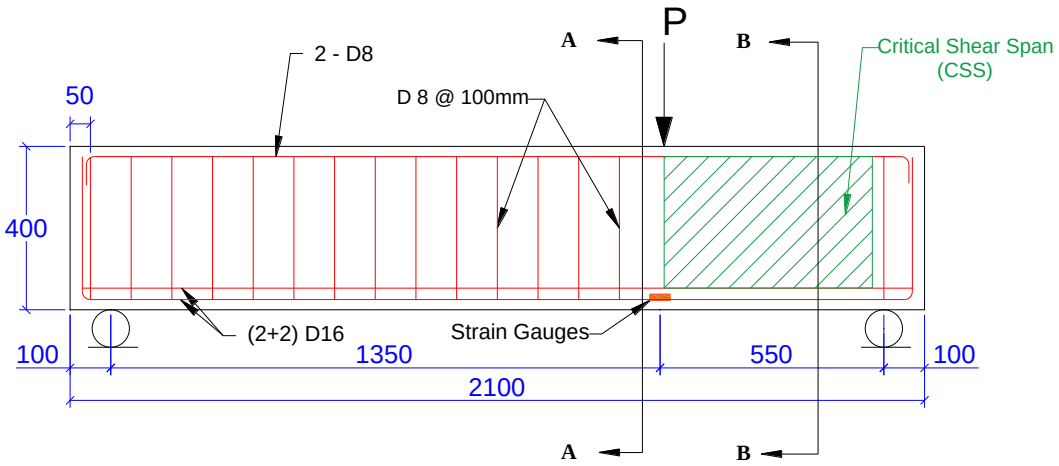

(a) Typical longitudinal section of the beam specimens

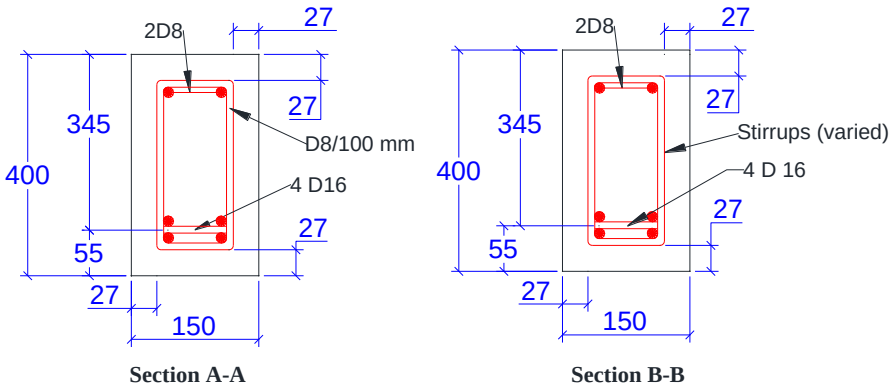

(b) Typical transverse cross sections

Figure 18: Typical beams specimen design.

Table 4:

Test Matrix of the Beam Specimens

No.	Designation	Strengthening technique	No. of EB/NSM-FRP	No. of stirrups in CSS	FRP/stirrups Interaction
1	R-S0	-	-	-	-
2	N2-S0	NSM	2	-	No stirrups
3	N3-S0	NSM	3	-	No stirrups
4	N4-S0	NSM	4	-	No stirrups
5	E2-S0	EB	2	-	No stirrups
6	E3-S0	EB	3	-	No stirrups
7	E4-S0	EB	4	-	No stirrups
8	R-S2-C1	-	-	2	-
9	N2-S2-C1	NSM	2	2	Aligned
10	E2-S2-C1	EB	2	2	Aligned
11	R-S2-C2	-	-	2	-
12	N2-S2-C2	NSM	2	2	Unaligned
13	E2-S2-C2	EB	2	2	Unaligned
14	R-S3-C1	-	-	3	-
15	N3-S3-C1	NSM	3	3	Aligned
16	E3-S3-C1	EB	3	3	Aligned
17	R-S3-C2	-	-	3	-
18	N3-S3-C2	NSM	3	3	Unaligned
19	E3-S3-C2	EB	3	3	Unaligned

Aiming to study the interaction between the steel stirrups and the FRP at the CSS, the specimens were designed to have five different stirrups configurations and three FRP configurations for each strengthening technique within the CSS. Overall, the investigated test parameters ware listed as follows:

i. A number of steel stirrups at the CSS: no stirrups, two stirrups with 200 mm spacing and three stirrups with 135 mm spacing.
ii. Strengthening technique: NSM and EB.
iii. Amount of FRP used to strengthen the beams: two, three and four EB/NSM FRP strips. Knowing that in the EB technique, the FRP strip has an area of (50 mm × 400 mm), while in the NSM technique, the same FRP strip (50 mm × 400 mm) has been cut into two slices (25 mm × 400 mm) and used together as double layers inside each groove.
iv. The interaction between steel stirrups and EB/NSM-FRP: aligned and unaligned.

For simplification, the designation of the specimens has been designed to provide a direct indication to the configurations of the FRP strengthening system, steel stirrups at CSS, and the relation between the steel stirrups and the FRP strengthening technique as listed in Table 4.

For the beam configuration, the nomenclature "R" denotes the reference beams that were kept unstrengthened; "N#" denotes the strengthened beams using NSM technique with "#" number of NSM-FRP; "E#" denotes the strengthened beams using EB technique with "#" number of EB-FRP strips.

For the steel stirrups configurations at the CSS, "S0" denotes to beams with no stirrups at the CSS; "S2" denotes the beams with two stirrups at the CSS; "S3" denotes the beams with three stirrups at the CSS. In order to differentiate between the beams with an aligned configuration and the beams with unaligned configuration, the nomenclature "C#" was used as follows: "C1" denotes the beams with aligned configuration between the steel stirrups and EB/NSM-FRP, and "C2" denotes the beams with unaligned configuration between the steel stirrups and EB/NSM-FRP.

The specimens were divided into three groups based on a number of the steel stirrups at the CSS:

Group 1: Consists of seven beam specimens have no steel stirrups at the CSS. Three beams were strengthened using NSM technique (2, 3 and 4 NSM-FRP). Three beams were strengthened using EB technique (2, 3 and 4 EB-FRP). One beam was kept unstrengthened for reference. See Figure 19.

Group 2: Consists of six beam specimens with two steel stirrups at the CSS. Two beams were strengthened with aligned FRP with the steel stirrups. Two beams were strengthened with unaligned FRP with the steel stirrups. Two beams were kept unstrengthened as references. See Figure 20.

Group 3: Consists of six beam specimens with three steel stirrups at the CSS. Two beams were strengthened with aligned FRP with the steel stirrups. Two beams were strengthened with unaligned FRP with the steel stirrups. Two beams were kept unstrengthened as references. See Figure 21.

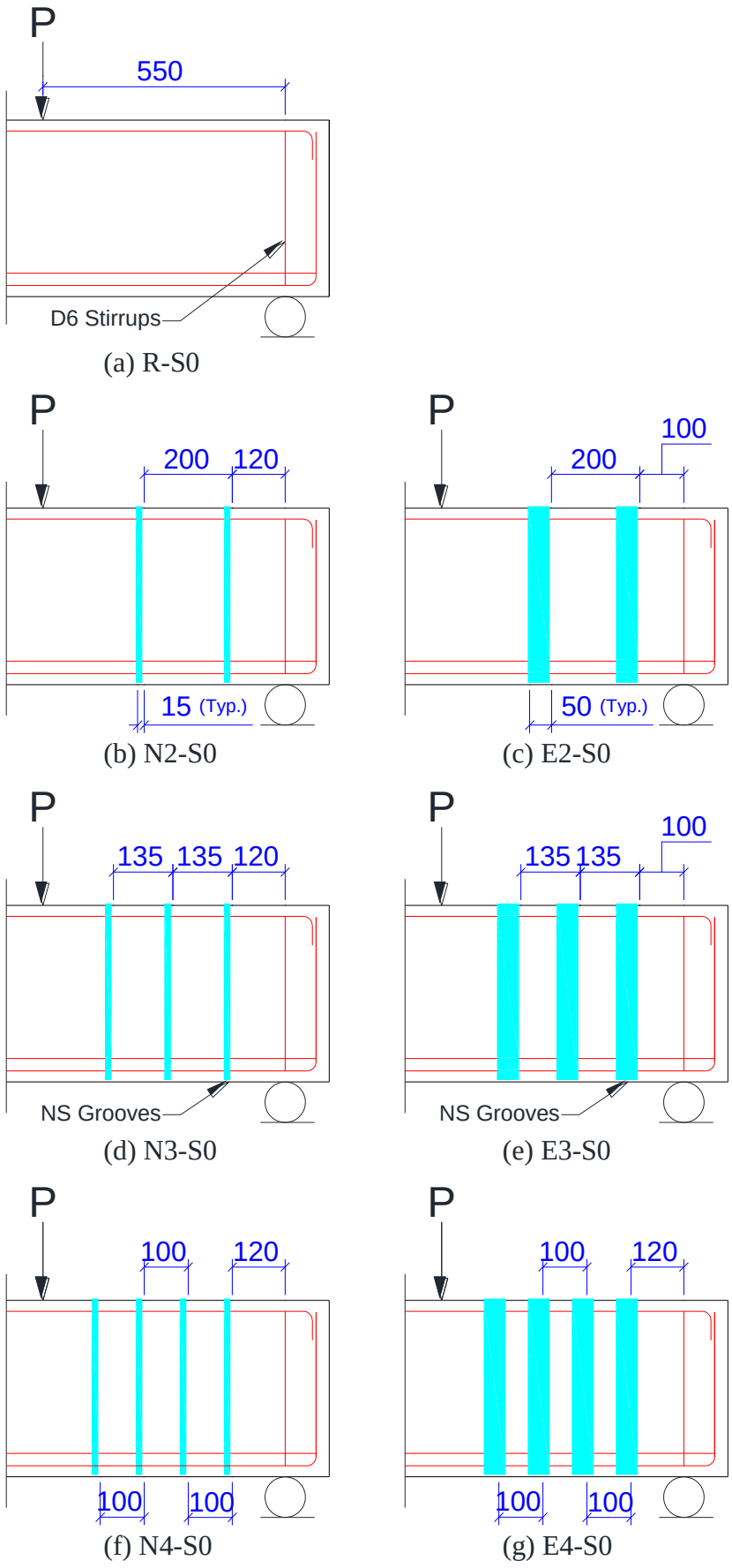

Figure 19: Group 1- Beam specimens with no stirrups at the CSS (Dimensions in mm).

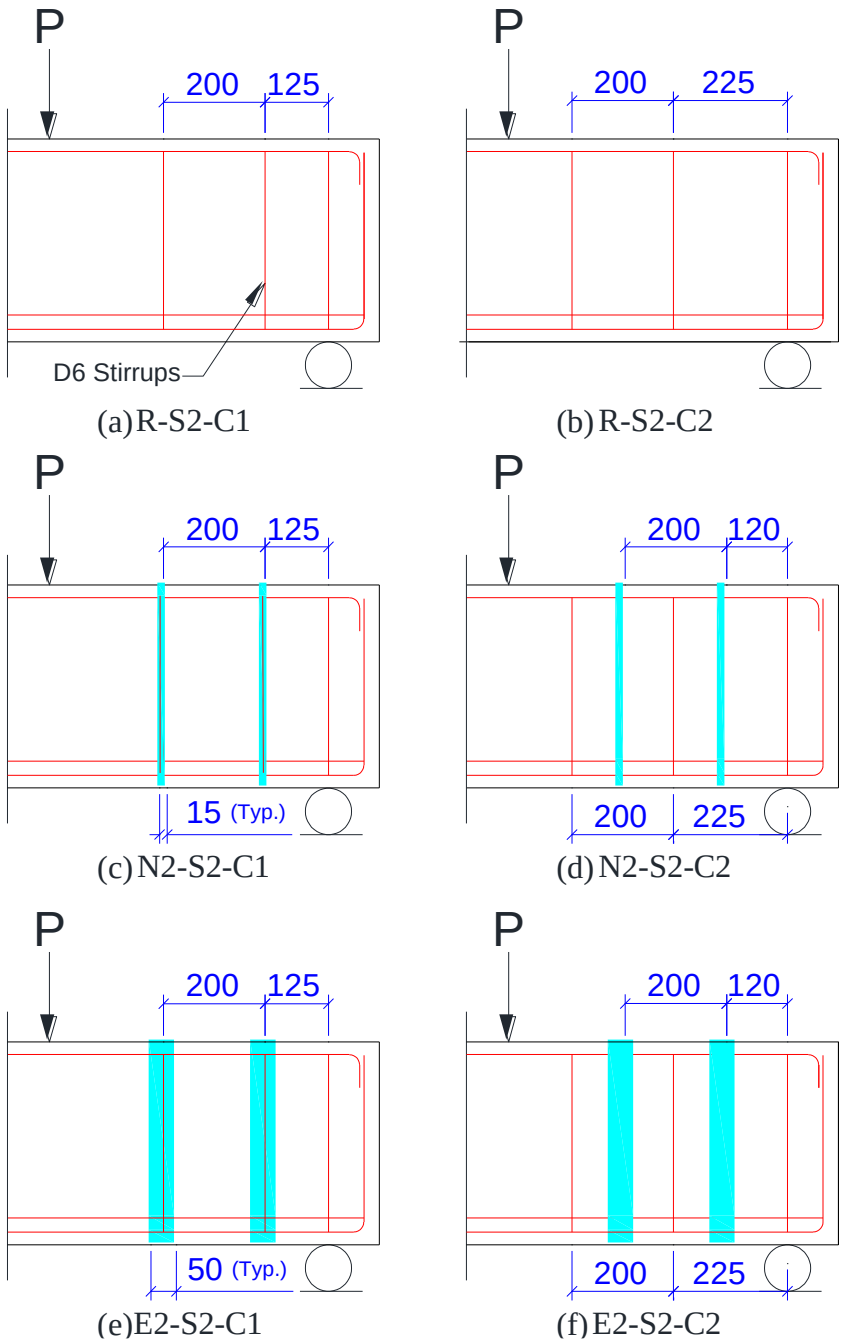

Figure 20: Group 2- Beam specimens with two stirrups at the CSS (Dimensions in mm).

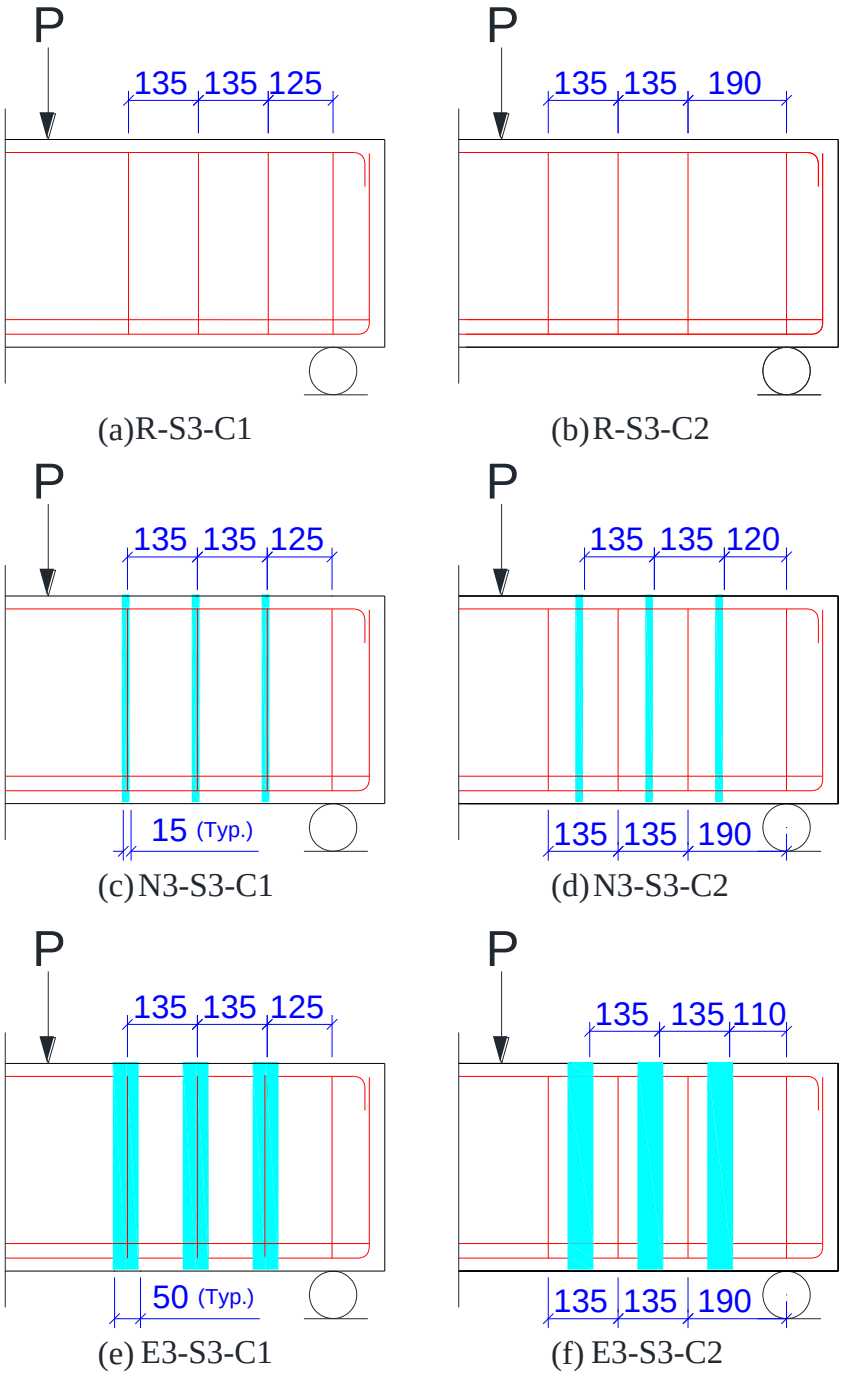

Figure 21: Group 3- Beam specimens with three stirrups at the CSS (Dimensions in mm).

3.3 Preparation of Beam Specimens

3.3.1 Steel Cage Preparation, Concrete Casting, and Curing

The preparation of the beam specimens is discussed in detail in this section. The preparation of the specimens has been performed according to the following steps:

1- Preparing the steel cage for each beam based on the design shop drawings.

2- Installing the strain gauges at the longitudinal steel bars and shear stirrups.

3- Fixing the steel cages inside a wood framework before concrete casting.

4- Casting the concrete for all beams, concrete cylinders, and concrete prisms.

5- Curing the specimens for at least 28 days.

The following sections provide more details for the beam's preparation process

3.3.1.1. Preparation of the steel cage and the strain gauges installation

Based on the design shop drawings, the bar bending schedule has been prepared and used to prepare the steel cages as shown in Figure 22.

Figure 22: Steel cages preparation.

The installation of the steel strain gauges for the longitudinal tensile reinforcement bars and shear stirrups within the CSS has been performed as follows:

1- Flipping the steel cage upside down to install the strain gauges for the longitudinal rebars (bottom reinforcements) as shown in Figure 23.
2- Grinding the bar surface at the location, where the strain gauge was installed.
3- Installing the strain gauge as suggested by the manufacturer, using a special type of super-glue.
4- Covering the strain gauges by electrical plastic tape for protection.

(a) Installation the strain gauge on the prepared surface in the flexure bars

(b) Cover the strain gauges by electrical tape for protection

Figure 23: Installation of steel strain gauges.

3.3.1.2. Preparation of formwork

The wooden formwork has been prepared in accordance with the designed beam dimensions as shown in Figure 24. It was essential to put a sign for every beam reinforcement configuration before casting to differentiate between them after concrete casting. Therefore, all beams with the same configuration were put together away from the others with a unique attached tag.

Figure 24: A wood framework for beam specimens.

3.3.1.3. Concrete casting and curing

After placing the steel cages into the prepared framework, the concrete casting was done as shown in Figure 25a through 25f. During the concrete casting, full supervision must be available to ensure proper concrete casting, continuous vibration process to prevent any air voids and well surface finishing for the beam specimens as shown in Figure 25c. The specimens were cured for a minimum of 28-days before application of the strengthening process as shown in Figure 25f.

(a) Concrete casting for beam specimens

(b) Concrete casting for cylinders and prisms

(c) Vibrating the concrete to avoid unwanted air voids

(d) Surface finishing

(e) Beams after surface finishing

(f) Curing for a minimum of 28 days

Figure 25: Concrete casting, surface finishing, and curing.

3.3.2 Strengthening Procedure for Beam Specimens

The strengthening procedure could be summarized as the following:

1- Cutting the FRP strips using a cutting machine as recommended by the manufacturer.

2- For NSM, grooves have been made on the concrete cover for the beam.

3- For EB, only little of sand plating has been made in the location, where the FRP strips were bonded.

4- Installing the FRP into the prepared grooves for NSM and bonding the FRP strips to the concrete cover surface for EB using epoxy as filling and bonding material for the NSM and EB techniques, respectively.

The following sections provide more details to the strengthening procedure.

3.3.2.1. Preparation of the FRP strips

As mentioned previously, the FRP is shipped by the manufacturer in rolls of length up to 30.5 m, width 100 mm and thickness 3.18 mm. FRP strips have been cut using the carpenter standard cutting machine as recommended by the manufacturer. FRP strips of dimensions 50 mm width and 400 mm length have been prepared for EB technique. FRP strips of dimensions 25 mm width and 400 mm length have been prepared for NSM technique as shown in Figure 26.

Figure 26: FRP strips cutting.

3.3.2.2. Application of NSM strengthening technique

After the beams become properly cured for at least four weeks, they were ready for NSM strengthening as shown for example in the illustration drawings Figure 27.

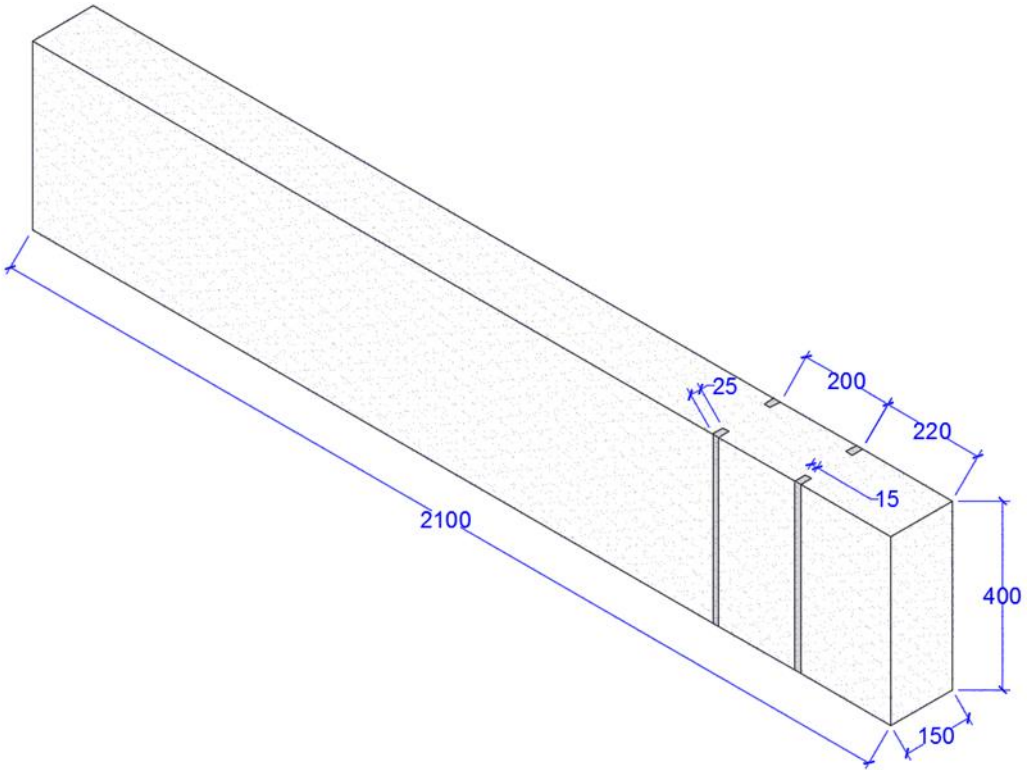

(a) Front view of a strengthened beam specimen

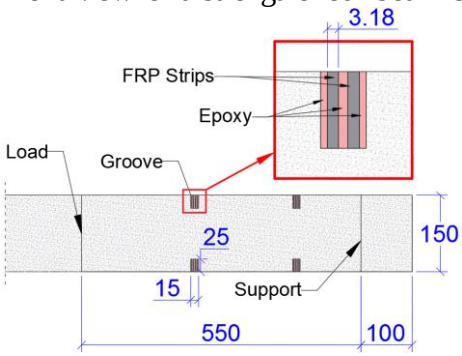

(b) Top view of strengthened beam specimens showing the typical NS-groove

Figure 27: Illustration drawing to show the NSM strengthening technique. Dimensions are in mm.

The following section introduces the procedure to apply the NSM technique to strengthen the beam specimens for shear.

A number of grooves were created at the CSS from both sides for each beam using HILTI DC-SE20 slitting machine based on the FRP configurations as shown in Figure 28. Each groove measures 15 mm wide, 25 mm deep and running along the beam height 400 mm. The grooves were cleaned from dust, debris, and any fine particles using a compressed air-brushing machine. Once all the grooves were prepared, installation of the FRP strips in the grooves started side by side for each beam. Figure 29a through 29e illustrate the installation of the FRP according to the following steps:

1- Approximately, half of the groove was filled by the epoxy as shown in Figure 29b.
2- Two FRP strips (25 mm x 400 mm) were completely covered by epoxy and attached allowing 2-3 mm layer of epoxy in-between as shown in Figure 29c.
3- This mass of FRP was placed inside the groove and lightly pressed to force the epoxy to flow around the FRP creating a layer of epoxy of 2-3 mm thickness from both sides of the FRP as shown in Figure 29d. This step was essential to ensure a full bond between the FRP and the concrete substrate.
4- The surface of each groove was leveled, and the excess of epoxy was removed.
5- Then, the same procedure (1-4) was followed on the other side of the CSS for each beam after leaving the epoxy to be hardened within 1-2 weeks.

Figure 28: HILTI DC-SE20 Slitting machine [75].

(a) Prepare the beam for strengthening

(b) Fill the ½ of the groove by epoxy

(c) Cover FRP strips by epoxy

(d) Insert the FRP strips in the groove

(e) The final shape of the beam specimens after NSM strengthening from one side.

Figure 29: NSM strengthening technique procedure.

3.3.2.3. Application of EB strengthening technique

After the beams become cured adequately for at least four weeks, they were ready for EB strengthening as shown for example in the illustration drawings Figure 30.

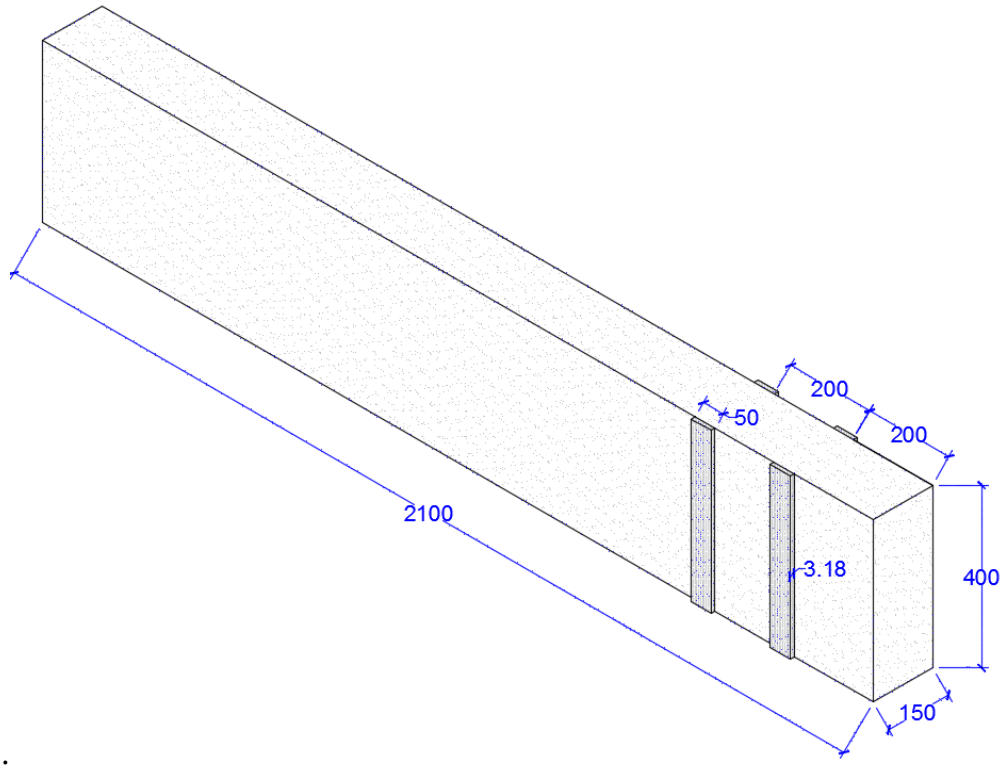

(a) Front view of a strengthened beam specimen

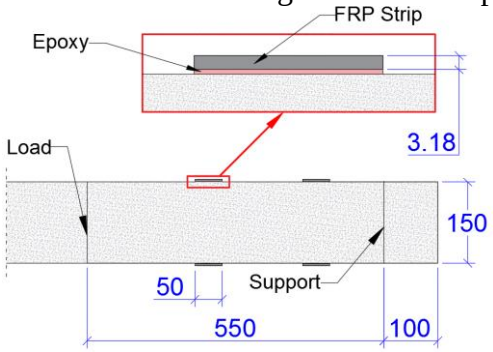

(b) Top view of a strengthened beam specimen showing the typical EB strip

Figure 30: Illustration drawing to show the EB strengthening technique.

The following steps illustrate the application of EB technique to strengthen the beam specimens for shear.

1- After adequate curing of the beam specimens, the locations in the CSS where the FRP strips were bonded have been marked based on the designed strengthening configuration.
2- Sandblasting for the marked locations has been done only at the locations of the FRP strips application as shown in Figure 31a.
3- The beams surface was cleaned adequately from dust, debris, and any fine particles using a compressed air-brushing machine as shown in Figure 31b.
4- A layer (epoxy 2-3 mm) has been applied to the beam surfaces at the specific locations as shown in Figure 31d.
5- One side of the FRP strips was covered by epoxy (2-3mm).
6- FRP strips are placed at their locations with a gentle press to ensure the whole FRP is bonded to the concrete surface using the epoxy. Adequate weights are placed over the FRP strips to prevent any movement of the FRP strips before epoxy become hardened as shown in Figure 31f and 31g.
7- Then, the same procedure (1-7) is followed on the other side of the CSS for each beam after leaving the epoxy to be hardened within 1-2 weeks.

(a) Sandblasting

(b) Clean the surface by compressed air

(c) A layer of epoxy on the FRP strip

(d) A layer of epoxy on the concrete surface

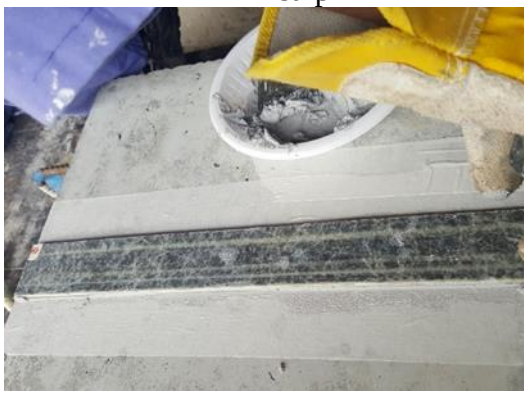

(e) Placing the FRP over the concrete

(f) Place a weight to fix the FRP in place

(g) Final shape after EB strengthening from one side of CSS

Figure 31: Procedure of EB strengthening technique.

3.4 Test Setup and Instrumentation

The beam test setup and the instruments used for data collection are described in Figure 32, which shows how the typical beam was placed in the loading frame with measuring devices and gauges. The beams were loaded by a controlled-displacement loading system that was applied under monotonically 3-point loading using (Instron 1500 HDX Static Hydraulic Universal) testing machine. The beams were loaded until failure at a rate of 0.25 mm/min.

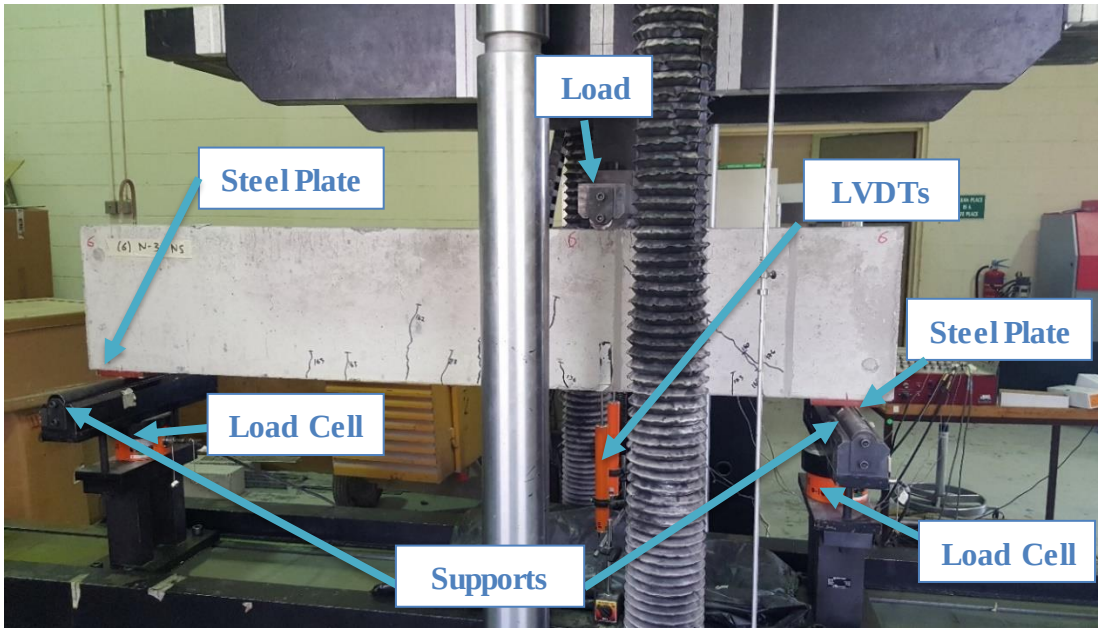

(a) The front side of the test beam setup

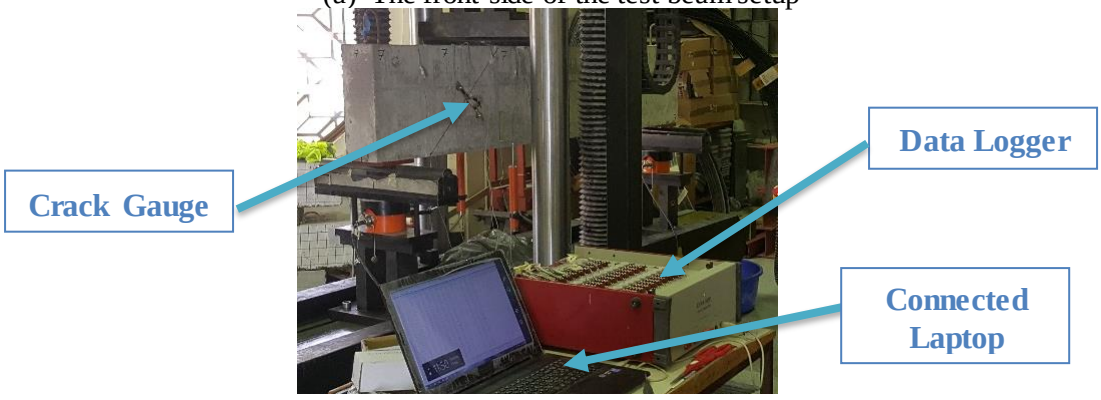

(b) The back side of the test beam setup

Figure 32: Beams test setup.

The loading machine is designed to calculate the load and the displacement continuously while loading. However, for extra confidence on the collected data, more devices were utilized to calculate the load and displacement at each beam. Two load-cells were placed under each support to calculate the actual load reactions for each loading step as shown in Figure 33. Also, two linear variable displacement transducers (LVDTs) were fixed under the loading point to monitor the actual displacement stepwise as shown in Figure 34.

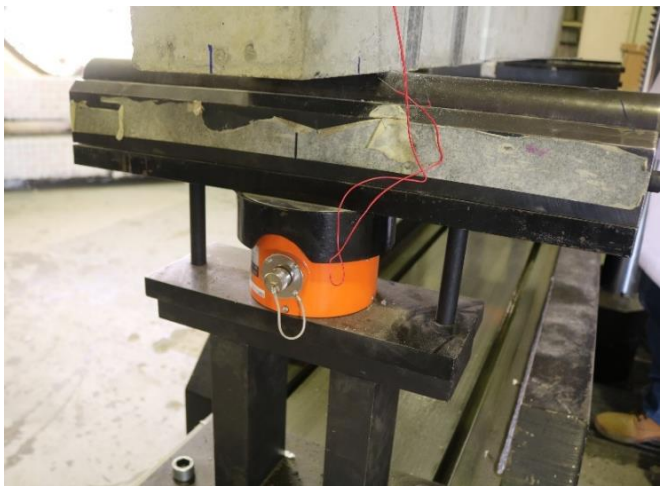

Figure 33: Load cell fixed under the support to monitor the reactions.

Figure 34: Linear variable displacement transducer (LVDT).

Additionally, the strains in the concrete surface and longitudinal tensile reinforcement were monitored using several types of strain gauges. For concrete strain monitoring, two PL-60-1 strain gauges of 60 mm length, 2% maximum strain limit and 120 Ω resistance were fixed on the concrete surface just below the loading point, as shown in Figure 36. For the longitudinal steel reinforcement strain monitoring, one FLA-5-11 strain gauge of 5 mm length, 2% maximum strain limit and 120 Ω resistance was fixed on each steel bar just below the loading point prior concrete casting. Also, the strain on the stirrups was monitored by installing FLA-5-11 strain gauge for all the steel stirrups at the CSS as shown in Figure 35.

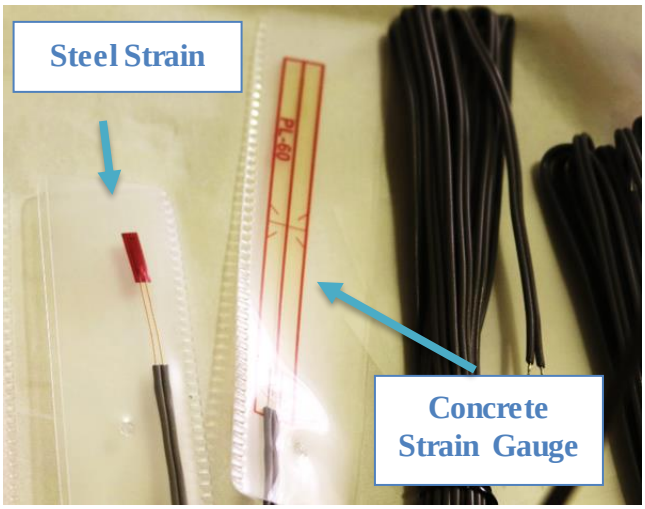

Figure 35: Strain gauges used for steel bars and concrete.

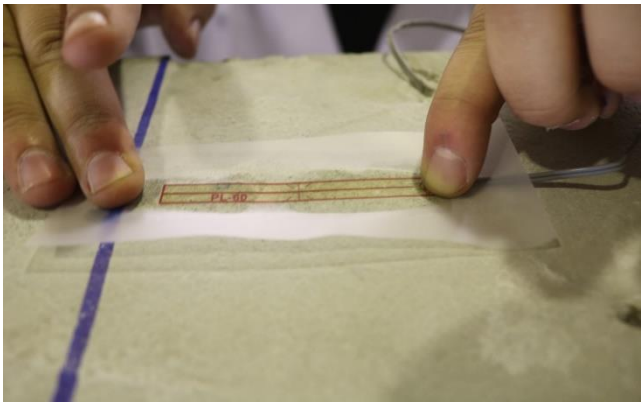

Figure 36: Installation of the concrete strain gauge.

Moreover, the crack width was monitored using a crack gauge (clip-type displacement transducer) of 5 mm capacity and 100 mm gauge length. The crack gauge was fixed perpendicular to the 45° line that was extended from the loading point to the bottom of the beams in order to catch the main failure crack as reported in the literature [76]. Furthermore, in order to prevent unnecessary stress concentrations, two steel plates of 25 mm thickness were placed at the supports. Generally, all the data which was collected from the strain gauges, crack gauges, and displacement transducers have been recorded using a data acquisition system (TML data logger) of a frequency 1 Hz as shown in Figure 37.

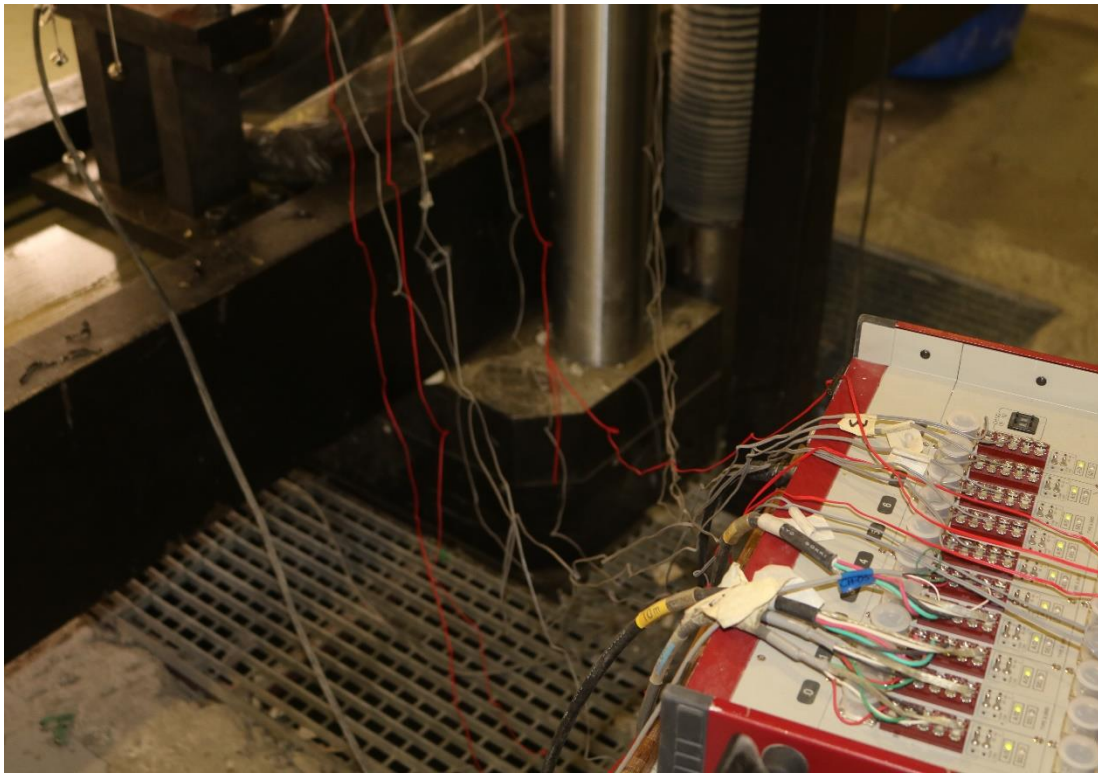

Figure 37: TML data logger used to collect the reading of all instrumentations.

CHAPTER 4: TEST RESULTS AND DISCUSSION

This chapter provides a detailed discussion of the observed results of all specimens during the experimental test.

The results of the specimens are discussed in terms of ultimate the load carrying capacity, the load-deflection response, the energy absorption, the strain analysis, the failure modes, and the crack propagation. Mainly, the research has been conducted to compare the contribution of each test parameter. Overall, the obtained results indicated the effectiveness of using both NSM and EB strengthening systems to enhance the shear capacity of RC rectangular deep beams. However, the NSM technique was found to have relatively better performance than that for EB technique.

A summary of the test results for the NSM and EB specimens with their associated references is given in Table 5. This table provides the observed results in terms of the ultimate load carrying capacity (P_u), the deflection at P_u (δ_u), the energy absorption (Ψ), the strain developed in flexural reinforcement at P_u ($\varepsilon_{sl,u}$), the maximum shear stirrups strain at P_u ($\varepsilon_{sv,u}$), the compressive strain developed in concrete at P_u ($\varepsilon_{c,u}$), the ultimate crack width CW at P_u, as listed in columns 2 through 8 respectively. Table 6 summarizes the contribution of the FRP strengthening systems in terms of the gain in P_u%, the gain in δ_u%, the gain in Ψ %, the strain developed in and the reduction in CW% as listed in columns 2 through 5 respectively.

Unfortunately, the crack width could not be monitored during the test for the EB strengthened specimens due to their common FRP debonding behavior, which can damage the crack gauges.

Table 5:

Summary of the Results

Specimen ID	P_u (kN)	δ_u (mm)	Ψ (kN.mm)	$\varepsilon_{sl,u}$ ($\mu\varepsilon$)	$\varepsilon_{sv,u}$ ($\mu\varepsilon$)	$\varepsilon_{c,u}$ ($\mu\varepsilon$)	CW (mm)
R-S0	224	6.3	741	2309	-	1060	1.537
R-S2-C1	257	7	949	2421	2881	1179	1.462
R-S2-C2	252	7.5	1072	2365	3363	1037	1.513
R-S3-C1	267	6.7	920	2573	2063	1491	1.561
R-S3-C2	263	6.1	817	2415	2408	1459	1.344
N2-S0	311	9.5	1720	3602	-	1115	0.986
N3-S0	337	8.9	1688	4216	-	1832	1.036
N4-S0	349	9.5	1839	-	-	1602	0.506
N2-S2-C1	331	8.7	1614	3465	2031	1548	0.986
N2-S2-C2	335	8.8	1621	4413	1343	1962	0.906
N3-S3-C1	369	17.9	4595	9998	1711	2662	0.963
N3-S3-C2	381	11	3129	7642	1411	2435	0.896
E2-S0	244	8.5	1069	2420	-	1824	-
E3-S0	257	8.7	1124	-	-	-	-
E4-S0	264	9.1	1224	-	-	-	-
E2-S2-C1	275	8.3	1293	2679	1501	2084	-
E2-S2-C2	267	8.1	1211	2841	1283	2724	-
E3-S3-C1	291	8.6	1330	2719	1301	2888	-
E3-S3-C2	282	8.5	1241	2843	1160	2907	-

Table 6:

Strengthening Contribution to the Specimens Results

Specimen ID	Gain in P_u (%)	Gain in δ_u (%)	Gain in Ψ (%)	Reduction in CW (%)
N2-S0	38.8	51.9	132.2	35.8
N3-S0	50.4	42.5	127.9	32.6
N4-S0	55.8	51.6	148.3	67.1
N2-S2-C1	28.8	24.0	70.0	32.6
N2-S2-C2	32.9	17.1	51.2	40.1
N3-S3-C1	38.2	165.9	399.4	38.3
N3-S3-C2	44.9	81.3	283.2	33.3
E2-S0	8.9	35.8	44.3	-
E3-S0	14.7	39.0	51.7	-
E4-S0	17.9	45.4	65.2	-
E2-S2-C1	7.0	18.1	36.3	-
E2-S2-C2	6.0	8.3	13.0	-
E3-S3-C1	9.0	28.0	44.6	-
E3-S3-C2	7.2	39.6	52.0	-

4.1 Test Results for Reference Specimens

This section introduces the results of the experimental test for the reference specimens in terms of the ultimate load carrying capacity P_u, deformational characteristics, crack width, strains at P_u, and modes of failure.

Overall, the load carrying capacity of the reference beams depended on the number of the shear stirrups at the CSS. The reference beam without shear stirrups R-S0 had the lowest load carrying capacity compared to the other reference beams. Likewise, there was no considerable difference between the load carrying capacity for the specimens with the same number of steel stirrups, e.g., specimens with two steel stirrups (R-S2-C1 and R-S2-C2), as well as specimens with three steel stirrups (R-S3-C1 and R-S3-C2).

The reference specimen without steel stirrups at the CSS (R-S0) exhibited a sudden shear failure caused by a major diagonal shear crack as shown in Figure 38. The ultimate load was recorded 224 kN for R-S0. The deflection of this specimen at the ultimate load was 6.3 mm. Energy absorption value of 741 kN.mm was observed for R-S0 at the ultimate load. The strains for the tensile steel bars and compression concrete were recorded as 2309 $\mu\varepsilon$ and 1060 $\mu\varepsilon$, respectively. Regarding the crack width, it did not exceed 1.6 mm for this specimens R-S0.

Figure 38: Crack pattern and failure mode for reference specimen, R-S0.

The reference specimens R-S2-C1 and R-S2-C2 were both designed to have two shear stirrups at the CSS with a spacing of 200 mm center-to-center. The only difference between these two reference beams was the location of the two steel stirrups in the critical shear span. Therefore, their results seemed to be remarkably close to each other. A load carrying capacity of 257 kN and 252 kN were recorded for R-S2-C1 and R-S2-C2, respectively. The ultimate deflection under the loading point was noticed to be in the range from 7 mm to 7.5 mm. Both specimens failed due to a major diagonal crack as shown in Figure 39a and 39b for R-S2-C1 and R-S2-C2, respectively. The crack width was observed around 1.5 mm for both specimens. The strain in the flexure bars was found to be around 2400 με for both specimens. However, the maximum strain in the shear stirrups was reported 2881 με and 3363 με for R-S2-C1, and R-S2-C2, respectively.

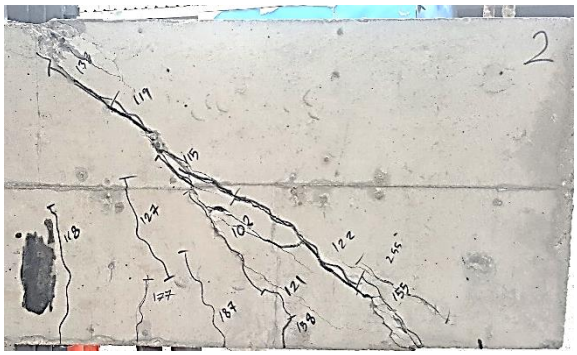

(a) R-S2-C1

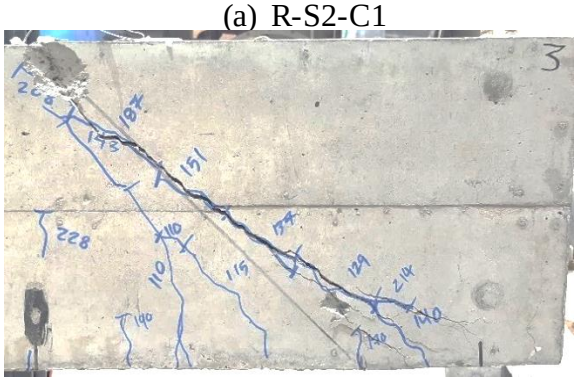

(b) R-S2-C2

Figure 39: Crack patterns and failure modes for specimens (a) R-S2-C1 and (b) R-S2-C2.

The reference specimens with three steel stirrups at the CSS (R-S3-C1 and R-S3-C2) were noticed to have an ultimate load of 267 kN and 263 kN before the sudden shear failure, respectively. These reference specimens had an average ultimate deflection of 6.4 mm. The strains in the flexure reinforcement were recorded 2573 με and 2416 με for R-S3-C1 and R-S3-C2, respectively. Both specimens exhibited a closed compression concrete strain around 1475 με. However, the maximum strain in the stirrups was reported to be 2063 με for R-S3-C1, and 2408 με for R-S3-C2. Specimen R-S3-C1 showed a crack width of 1.6 mm, while that was 1.3 mm for the specimen R-S3-C2 at the ultimate load. The shear mode of failure and the crack pattern of both specimens R-S3-C1 and R-S3-C2 are presented in Figure 40a and 40b, respectively.

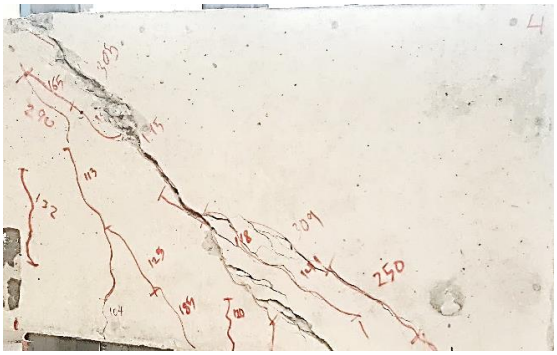

(a) R-S3-C1

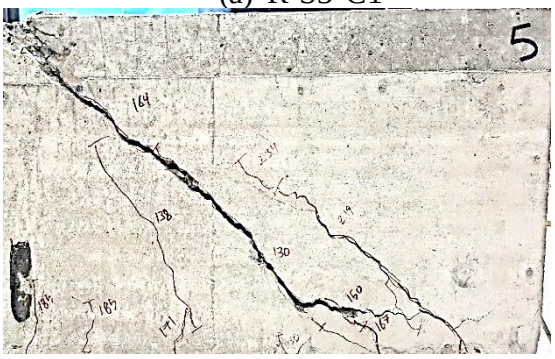

(b) R-S3-C2

Figure 40: Crack patterns and failure modes for specimens (a) R-S3-C1 and (b) R-S3-C2.

4.2 Test Results for NSM Specimens

In this section, the results of the NSM strengthened specimens are discussed. Total of seven specimens was strengthened using NSM technique. Three FRP configurations were tested; namely, 2, 3 and 4 NSM-FRP at the CSS. Each NSM-FRP groove contains two layers of FRP strips (25 mm × 400 mm) bonded together with epoxy and covered from all sides by epoxy as explained in chapter 3. Overall, the steel configurations ware found to play a dominating role in the FRP contribution. Three steel configurations have been studied; namely, no stirrups, stirrups aligned with the NSM-FRP and stirrups unaligned with NSM-FRP. The results are discussed in the following sections in terms of the ultimate load carrying capacity, the load-deflection response, the energy absorption, the strain analysis, the modes of failure and the crack propagation.

4.2.1 Ultimate Load Carrying Capacity

The ultimate load carrying capacity of each NSM strengthened specimen and the percentage of gain in P_u relative to the associated reference specimens are given in the second columns of Table 5 and 6, respectively. The NSM strengthening system showed a significant increase in the P_u with a gain percentage ranged from 28.8% to 55.8%, relative to the corresponding reference specimens. This indicated the successful of the NSM application for the shear strengthening of RC deep beams. However, the effectiveness of the strengthening system varied based on the tested parameters.

Specimens with steel stirrups at the CSS has found to have lower gain in the shear capacity. To illustrate, by comparing the beams with two NSM-FRP, the gain percentage of the load carrying capacity reached 38.8% for the specimen without shear stirrups (N2-S0) and only 28.8% and 32.9% for the beams with shear stirrups N2-S2-C1 and N2-S2-C2, respectively.

Equivalently, the specimen with three NSM-FRP and no shear stirrups (N3-S0) was able to enhance the load capacity by 50.4%, while the beams with the same amount of FRP but with shear stirrups (N3-S3-C1 and N3-S3-C2) could not increase the load carrying capacity by more than 38.2% and 44.9%, respectively. Figure 41 shows the gain in P_u % for all the NSM strengthened beams. As shown in Figure 41, the gain in P_u % for specimens without stirrups is relatively higher than that gain for specimens with steel stirrups at the CSS.

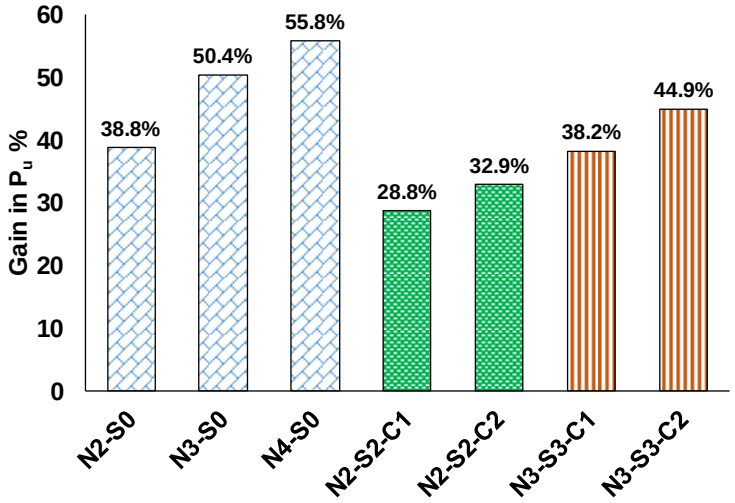

Figure 41: Gain in Pu % for NSM strengthened specimens.

By comparing the strengthened specimens with no steel stirrups at CSS, it was observed that the more NSM-FRP were used, the higher the loading carrying capacity was recorded for each specimen. Particularly, a strengthened specimen with four NSM-FRP experienced the highest load carrying capacity of 349 kN, while that was 337 kN and 311 kN for the strengthened specimens with three and two NSM-FRP, respectively. Correspondingly, the gain in P_u% was found to be significantly increased, as the number of used FRP increased.

To elaborate further, the specimen N4-S0 showed an increase in the load carrying capacity of 55.8%, while that increase was 50.4% and 38.8% for the specimens N3-S0 and N2-S0, respectively and compared to the reference beam R-S0. Figure 42 shows how the gain in P_u % was gradually decreased as the amount of used NSM-FRP was reduced.

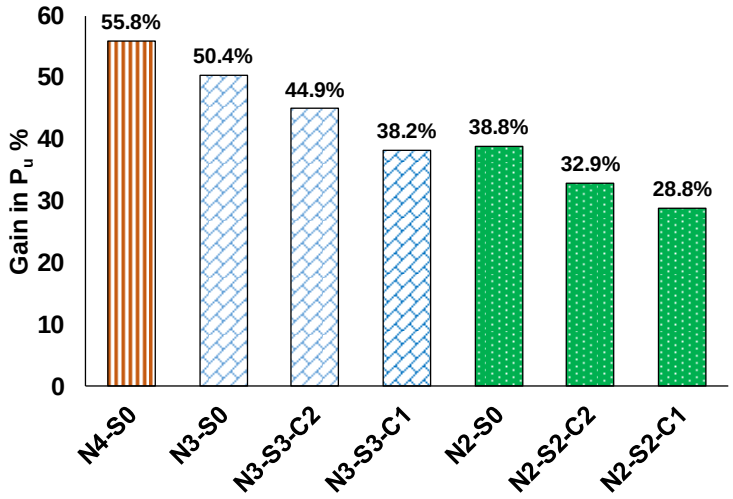

Figure 42: Gain in P_u % comparison in terms number of NSM-FRP.

The interaction between the steel stirrups and the NSM-FRP at CSS was one of the main study's objectives. Admittedly, shear stirrups at the CSS reduced the FRP contribution on the load carrying capacity as mentioned previously. However, the impact of the relation between the steel stirrups and the NSM-FRP could be reported as follows. Specimens with unaligned configuration were observed to have higher load carrying capacity than that for the specimens with aligned configuration. This observation indicates the effectiveness of placing NSM-FRP unaligned to the steel stirrups. In numbers, the beam with three NSM-FRP and three steel stirrups unaligned to each other (N3-S3-C2) reached load carrying capacity up to 381 kN, while the beam with the same amount of FRP and steel stirrups but aligned to each other (N3-S3-C1) could not reach more than 369 kN.

Similarly, comparing the beams that have been strengthened using two NSM-FRP, it was remarked that the beam with aligned configuration (N3-S3-C1) showed an increase in the load carrying capacity of 28.8%, while the beam with unaligned configuration (N3-S3-C2) was able to enhance the load carrying capacity up to 32.9%. Figure 43 shows the gain in P_u % for the aligned configuration (red color) and the unaligned configuration (blue color) for NSM strengthened specimens.

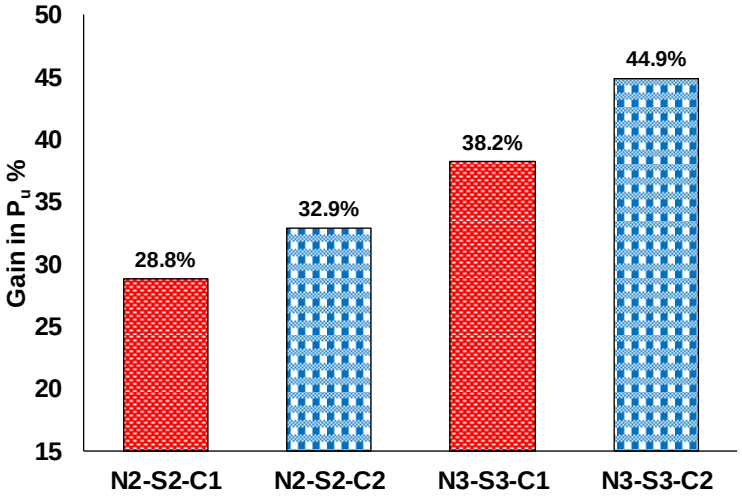

Figure 43: Gain in P_u % for aligned configuration verses unaligned configuration.

4.2.2 Load-Deflection Response

The reference beams experienced remarkable lower ultimate deflections than that for the strengthened beams, as shown in Table 5 and 6. This can be an indication of the NSM technique's efficacy to enhance the ductility behavior of RC deep beams. Overall, the gain % in the deflection for the strengthened specimens has been listed in the third column of Table 6. The average ultimate deflection for reference beams was 6.7 mm, while that was 10.6 mm for the NSM strengthened beams, with difference percentage 58.1%. This explained the effectiveness of the strengthening technique to enhance the ductility of the deep beams which are known to have brittle behavior.

Through studying the behavior of the NSM strengthened beams without shear stirrups at the CSS, it was observed that the ultimate deflection values ranged from 8.9 mm to 9.5 mm with an average of 9.3 mm. Correspondingly, the increase % in the ultimate deflection for specimens without steel stirrups at the CSS was reported from 42.5% to 51.9% with an average of 48.7%. The lowest ultimate deflection was observed at the specimen N3-S0 (δ = 8.9 mm), while the highest ultimate deflection was obtained at the specimens N4-S0 (δ = 9.5 mm). Correspondingly, strengthened specimen using two NSM-FRP was noticed to increase the ultimate deflection by 51.9 %, while an increase in the ultimate deflection of 42.5% and 51.6% were achieved using three and four NSM-FRP, respectively.

Highlighting the results of the specimens strengthened using three NSM-FRP, it was observed that they had the highest ultimate deflection. These specimens showed a significant increase in the ultimate deflection; up to 165.9% compared to the corresponding reference specimens. The average increase in the ultimate deflection was 96.6% of specimens with three NSM-FRP. Specimens with aligned configuration between the steel stirrups and the NSM-FRP were noticed to have relatively higher ultimate deflection than that with unaligned configuration. Particularly, the beam with the aligned configuration between the steel stirrups and NSM-FRP showed the largest ultimate deflection (δ = 17.9 mm).

Regards the specimens with two NSM-FRP, the ultimate deflection ranged from 8.7 mm to 9.5 mm with an average of 9 mm. The highest gain percentage on the ultimate deflection for specimens with two NSM-FRP was credited 51.9% for the specimen N2-S0. However, the specimens N2-S2-C1 and N2-S2-C2 showed an increase in the ultimate deflection of 24% and 17.1%, respectively, as shown in Figure 44.

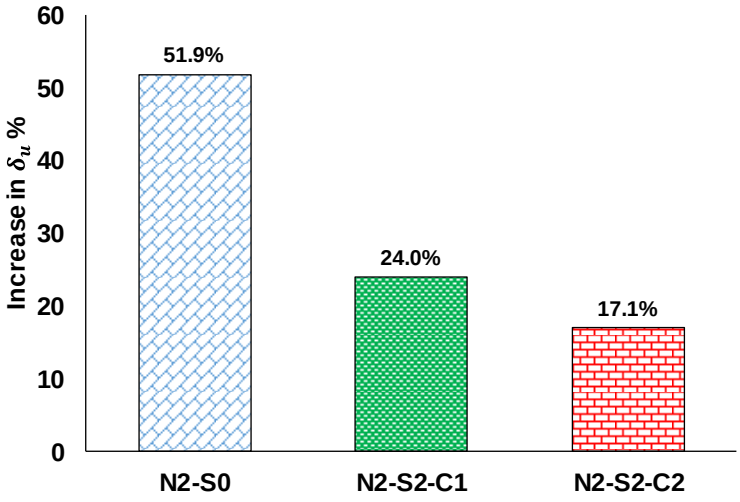

Figure 44: Ultimate load deflection for specimens with two NSM-FRP.

Figure 45a shows the load-deflection plots for specimens with no steel stirrups, while Figure 45b and 45c present the load-deflection plots for specimens with two and three steel stirrups at the CSS, respectively. By studying these load deflection graphs, it can be noticed that the specimens with the same strengthening behaved similarly with a small difference at the peak point. Additionally, as expected due to the common compression shear failure mode, most of the specimens experienced a sudden drop in the load-displacement curve at the failure point. However, specimen N3-S3-C1 exhibited a unique behavior at the peak point due to experiencing more flexural resistance before the completed rupture in compression shear failure as shown in Figure 45c.

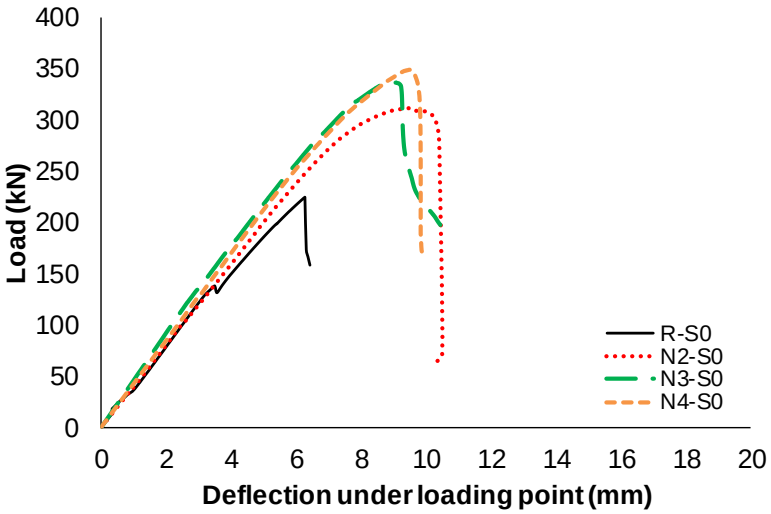

(a) Specimens with no steel stirrups at the CSS

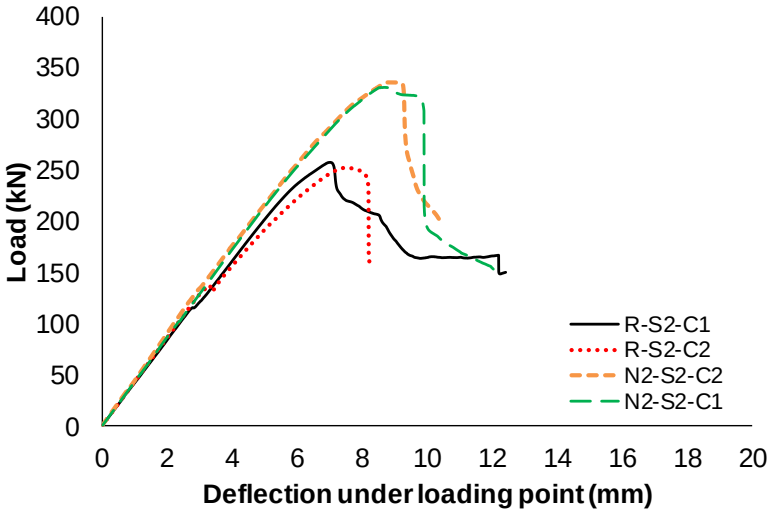

(b) Specimens with two steel stirrups at the CSS

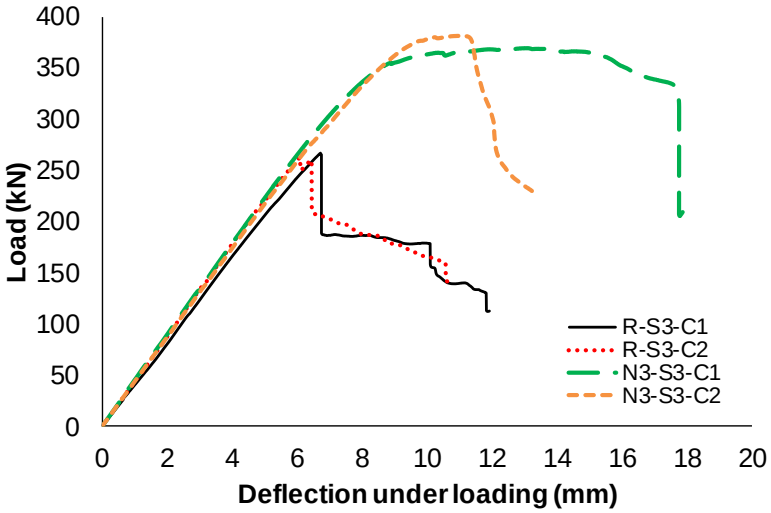

(c) Specimens with three steel stirrups at the CSS

Figure 45: Load-deflection plots for NSM strengthened specimens.

4.2.3 Energy Absorption

The energy absorption is the area under the load-deflection curve [77]. The energy absorption for each specimen has been listed in Table 5. Generally, the NSM strengthening technique increased energy absorption. The increase % of the strengthened specimens was listed in the fourth column of Table 6.

The energy absorption for the reference beams ranged from 741 kN.mm to 1072 kN.mm with an average of 900 kN.mm. For the strengthened specimens, the energy absorption ranged from 1614 kN.mm to 4595 kN.mm, with an average of 2315 kN.mm. This corresponds to an average increase of 173.2% in the energy absorption for all NSM strengthened specimens. Figure 46 shows the energy index (Ψ/Ψ_R) for specimens with two and three steel stirrups at the CSS. The aligned configuration showed slightly higher energy index than that for the unaligned configuration as shown in the Figure 46. Additionally, the specimens with three steel stirrups and three NSM-FRP exhibited much higher energy index than that for the specimens with only two steel stirrups and two NSM-FRP at the CSS.

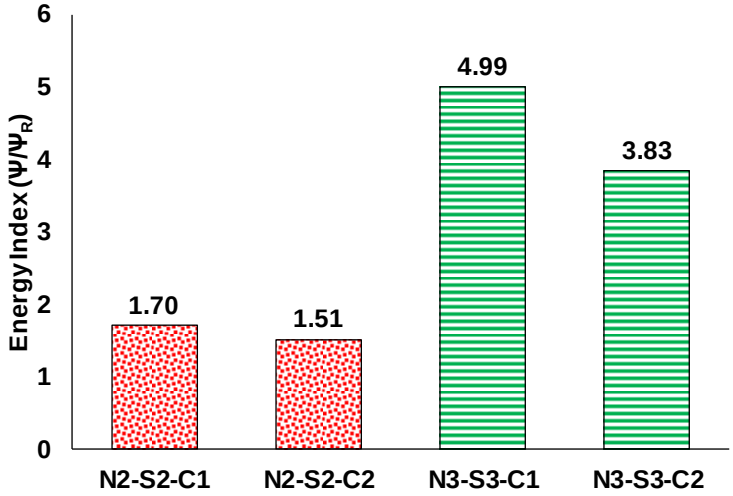

Figure 46: Energy index for three and two NSM-FRP strengthened specimens.

4.2.4 Strain Analysis

4.2.4.1. Tensile reinforcement strain

As mentioned previously, four 16 mm diameter steel bars (double layer) were used as a typical tensile reinforcement for all beam specimens. Two strain gauge was installed on the bottom steel bars to monitor the flexural strain during the experimental test. Both bars should have approximately the same strain reading due to the symmetric geometry of the beam. However, sometimes one of the strain gauges or both of them could be damaged during the concrete casting process. This what happened to the specimen N4-S0.

The strengthened specimens showed much higher flexural strain than that for the reference specimens as the average difference exceeded 128%. The ultimate steel strain was reported for the NSM strengthened specimens in the range from 3465 με to 9998 με with an average 5523 $\mu\varepsilon$. Correspondingly, the increase % in the flexural strain for the strengthened specimens ranged from 43.1% to 288.6% with an average of 129%. This can be referred to the two specimens (N3-S3-C1) and (N3-S3-C2), which have experienced relatively more flexural bending during the experimental test.

Generally, the strengthened specimens with two NSM-FRP were found to have lower tensile strain than that for the specimens with three NSM-FRP. The average increase in the flexural strain for specimens with two NSM-FRP was observed 64.9%, while that was 195.9% for the specimens with three NSM-FRP.

Figure 47a shows the load-strain curves of the flexure reinforcement for the specimens without steel stirrups at the CSS. However, Figure 47b and 47c show the load-strain curves of the flexure reinforcement for specimens with two and three steel stirrups at the CSS, respectively. As shown in Figure 47a the more FRP used the higher the ultimate flexural stain. From Figure 47b, it can be observed that although both

strengthened specimens exhibited approximately the same ultimate load, the specimen N2-S2-C1 showed more elastic behavior than that for the specimen N2-S2-S2. From Figure 47c, it was clear that the specimens N3-S3-C1 and N3-S3-C2 have been noticed to enter into a partial flexure failure before the rupture point. This attributed to the success of the strengthening technique, that was able to increase the shear strength of the specimen quite enough to make the deep beam to start failing in flexure before its typical compression shear failure.

4.2.4.2. Concrete strain

The compression strain of the concrete has been monitored during the test using two strain gauges, that were fixed on the concrete surface underneath the loading point.

Generally, the ultimate concrete strain that corresponded to the ultimate load for all the strengthened specimens had never exceeded the typical concrete crushing strain 3500 $\mu\varepsilon$. The average of the concrete strain for the reference specimens was found 1245 $\mu\varepsilon$, while that was 1879 $\mu\varepsilon$ for the strengthened specimens. This has resulted in an average increase in the concrete strain of 56.4% due for the all NSM strengthened specimens. It was also observed that the greater number of FRP used for strengthening, the higher concrete compression strain was remarked. The average gain percentage in the concrete strain was reported 41.9% for beams with two NSM-FRP, and 72.8% for beams with three NSM-FRP.

Regards the beams with no shear stirrups in the CSS, they were found to have the lowest increase in the ultimate concrete strain. The average ultimate concrete strain was observed 1402 $\mu\varepsilon$, and the average increase in the concrete strain was determined 43.1% for all the strengthened beams without steel stirrups.

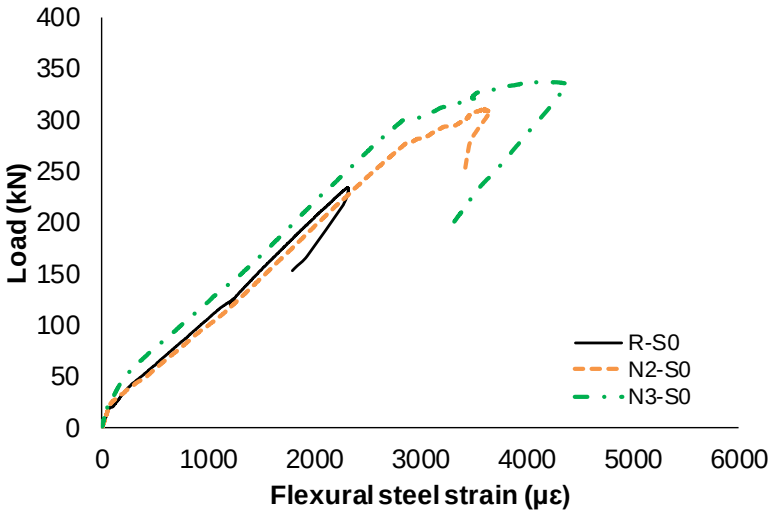

(a) Specimens with no steel stirrups at the CSS

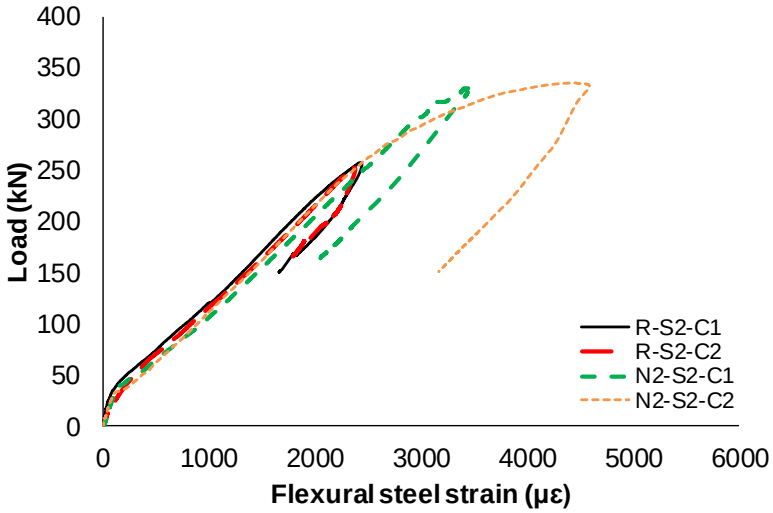

(b) Specimens with two steel stirrups at the CSS

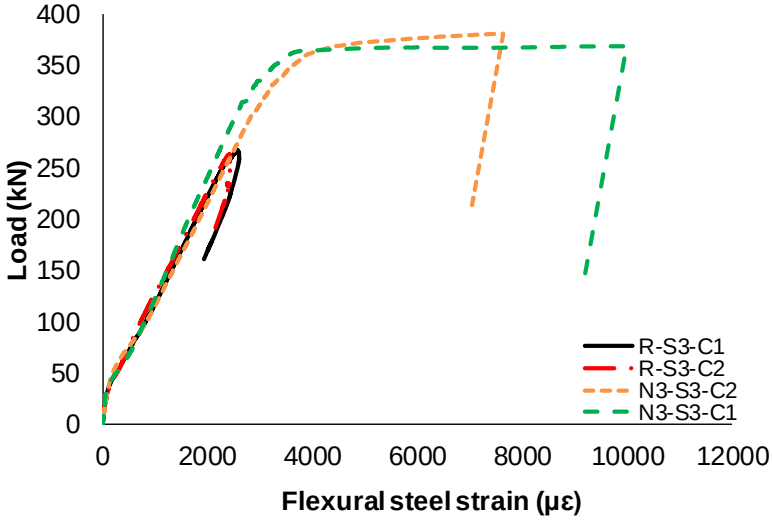

(c) Specimens with three steel stirrups at the CSS

Figure 47: Load-flexure steel strain plots for NSM strengthened specimens.

Moreover, the interaction between the steel stirrups and the NSM-FRP was found to have a dominating role in the concrete strain of the beams. The beams with aligned configuration were noticed to have a much lower increase % in the concrete strain than that for the unaligned configuration. The average gain percentage of the ultimate concrete strain was observed 54.9% for aligned configuration beams, while that was 78% for the unaligned configuration beams.

4.2.4.3. Stirrups strain

Total of four specimens with steel stirrups at the CSS has been strengthened using NSM technique. Therefore, four specimens with steel stirrups at the CSS were kept unstrengthened to act as references. Overall, the strengthening technique significantly reduced the strain of the steel stirrups. This attributed to the efficacy of the FRP strips to resist some of the total applied shear stresses. In other words, FRP strips and steel stirrups work together to reinforce the beam against the applied shear stresses. The maximum stirrups strain for each specimen has been listed in Table 5.

The average strain of stirrups for the reference specimens was observed 2679 $\mu\varepsilon$, while that was 1695 $\mu\varepsilon$ for the NSM strengthened specimens. However, it also noticed that specimens with aligned configuration were able to reduce the strain in the stirrups more than that for the specimens with aligned configuration. The average decrease in the strain of stirrups for specimens with unaligned configuration reached 51%, while that for specimens with aligned configuration did not exceed 23.3%.

4.2.5 Failure Modes and Crack Propagation

Overall, the entire specimens failed due to a major diagonal shear crack as shown in Figure 48a through 48g. Some specimens were noticed to have a partial separation of the concrete cover around the NSM-FRP at the beams' bottom as shown in Figure 49a through 49g. During the experimental test of the specimen N2-S2-C2, a piece of concrete has been suddenly jumped away from the beam corner as shown in Figure 50.

Specimens with three NSM-FRP and three steel stirrups at the CCS (N3-S3-C1 and N3-S3-C2) have entered into a partial flexure failure mode before the completed compression shear failure. This indicates that the NSM shear strengthening system was effective enough to change the typical behavior of the RC deep by failing in flexural-shear instead of failing directly in shear. However, the diagonal shear cracks were still noticed for both beams as shown in Figure 48g and Figure 48f for specimen N3-S3-C1 and N3-S3-C2, respectively. Moreover, a relatively extensive concrete crushing under the loading point was noticed in these specimens N3-S3-C1 and N3-S3-C2 as shown in Figure 51.

The crack width has been monitored using a clip-type displacement transducer, that was fixed on the expected location of the main failure crack. Typically, this location is to be along a line of 45-degree extended from the loading point to the bottom of the beam. The crack gauge is fixed perpendicular to this line in order to measure the crack propagation at each loading step. The ultimate crack width, which was recorded at the ultimate load, is listed for all specimens in Table 5.

In general, the reference specimens were found to have much higher crack width than that for the strengthened specimens. In other words, the utilization of the FRP to strengthen the shear capacity of the RC deep beams has a dominating role in reducing the ultimate crack width.

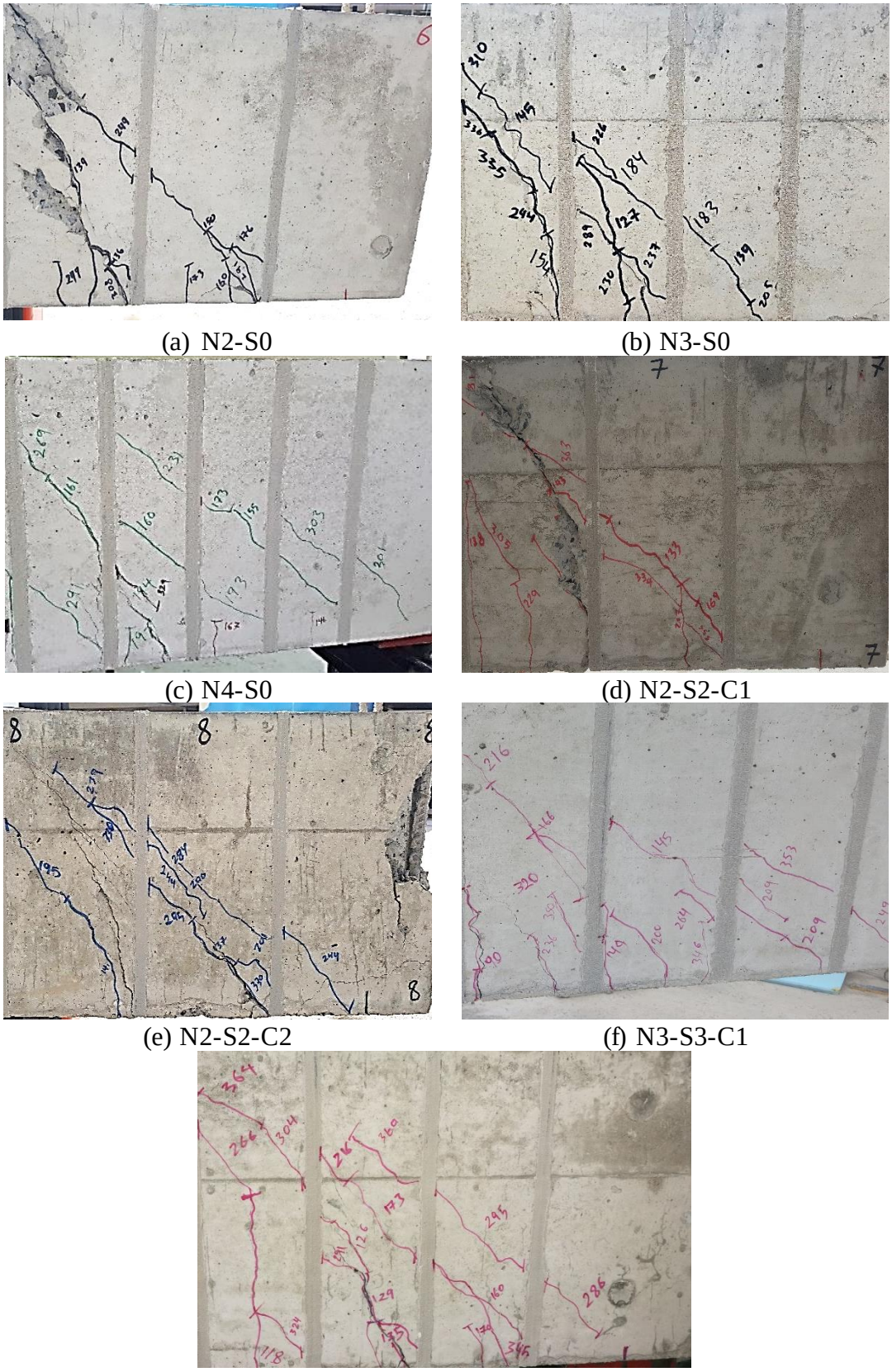

(a) N2-S0 (b) N3-S0

(c) N4-S0 (d) N2-S2-C1

(e) N2-S2-C2 (f) N3-S3-C1

(g) N3-S3-C2

Figure 48: Crack pattern and failure mode for NSM specimens (Front view).

(a) N2-S0

(b) N3-S0

(c) N4-S0

(d) N2-S2-C1

(e) N2-S2-C2

(f) N3-S3-C2

(g) N3-S3-C1

Figure 49: Bottom cracks and concrete debonding for NSM specimens.

Figure 50: Broken concrete mass while testing the specimen N2-S2-C2.

Figure 51: Concrete crushing under the loading point for specimens N3-S-C2/C1

The reduction percentage of the crack width for the strengthened specimens was listed in the last column of Table 6. The average crack width for the reference specimens was observed around 1.5 mm, while that was only 0.9 mm for the strengthened specimens. There was no considerable difference in the crack width between the specimens with two and three steels stirrups at the CSS. However, the unaligned configuration exhibited lower crack width than that for the aligned configuration.

Figure 52a shows the load-crack width plots for specimens without steel stirrups, while Figure 52b and 52c show the load-crack width plots for specimens with two and three steel stirrups at the CSS, respectively. From Figure 52a, it can be noticed that increasing the number of NSM-FRP, with the absence of steel stirrups, significantly reduced the ultimate crack width. From Figure 52b, it was remarked that at the same load, the specimen with unaligned configuration (N2-S2-C2) had less crack width than that for the specimen with aligned configuration (N2-S2-C1). However, this was not the case for the specimens with three NSM-FRP and three steel stirrups at CSS. Particularly, as shown in Figure 52c, there was no considerable difference between the specimens with aligned and unaligned configurations, especially at the beginning of the test.

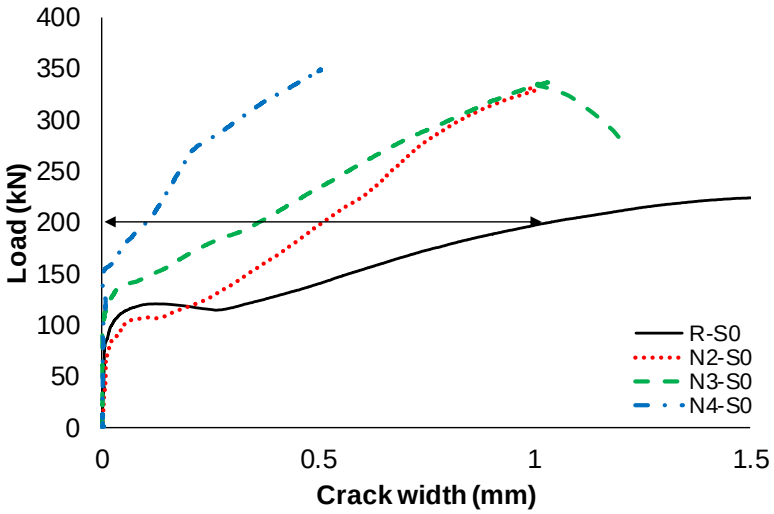

(a) Specimens with no steel stirrups at the CSS

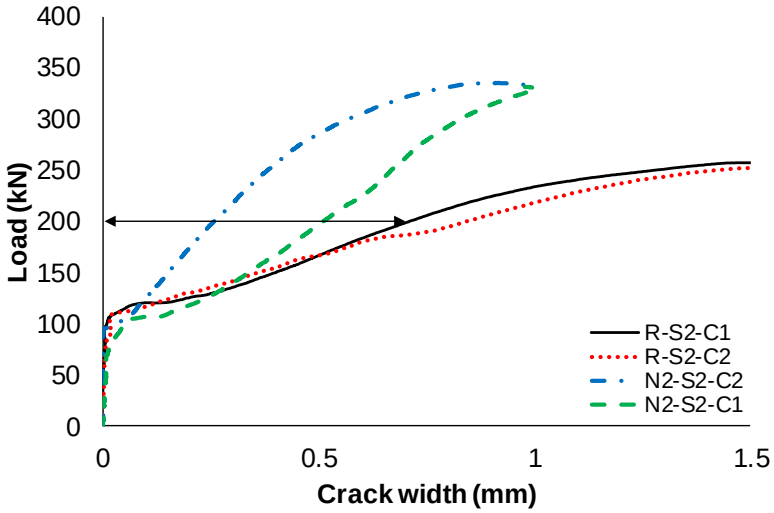

(b) Specimens with two steel stirrups at the CSS

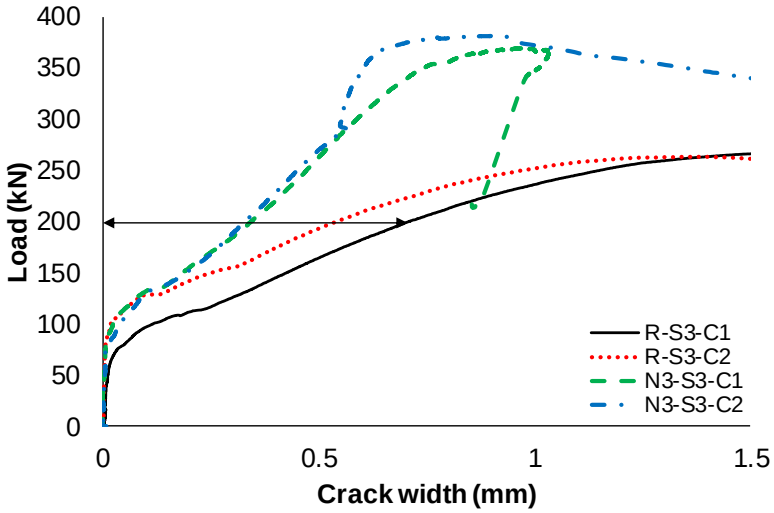

(c) Specimens with three steel stirrups at the CSS

Figure 52: Load-crack width plots for NSM strengthened specimens.

4.3 Test Results for EB Specimens

In this section, the results of the strengthened specimens using EB technique are discussed in terms of the ultimate load carrying capacity, load-deflection response, energy absorption, strain analysis, and failure modes. Similar to the NSM technique, there was three FRP configuration on the EB technique; namely, (2, 3 and 4 EB-FRP). Each EB-FRP strip has a dimension of 50 mm wide and 400 mm length. Thus, the area of each EB-FRP strip is equal to the total area of one NSM-FRP. Overall, the results showed success of the EB technique to enhance the shear capacity of the RC deep beams, but not as well as NSM technique. The same reference specimens were used to assess both NSM and EB techniques.

4.3.1 Ultimate Load Carrying Capacity

The ultimate load carrying capacity of each EB strengthened specimen and the gain in P_u% relative to the associated reference specimens are given in the second columns of Table 5 and 6, respectively. Generally, the strengthening system showed an increase in P_u with gain, percentage ranged from 6% to 17.9% relative to the reference specimens. This indicated an acceptable success of the EB application for the shear strengthening of RC deep beams. The effectiveness of the strengthening system varied based on the tested parameters.

The presence of the shear stirrups at the CSS has found to decrease the contribution of the EB-FRP. To illustrate, by equating the specimens that were strengthened using two EB-FRP, it was noticed that the gain percentage of the load carrying capacity reached 8.9% for the specimen E2-S0, while that ratio was 6% and 7% for the specimens E2-S2-C2 and E2-S2-C1, respectively.

Equivalently, the specimen with three EB-FRP and without shear stirrups showed an enhance in the loading capacity of 14.7%, while that ratio was 9% and 7.2% for the specimens with the same amount of EB-FRP but with shear stirrups. As shown in Figure 53, the gain in P_u % for specimens without stirrups is relatively higher than that for specimens with steel stirrups at the CSS. This behavior was noticed the same using the NSM technique.

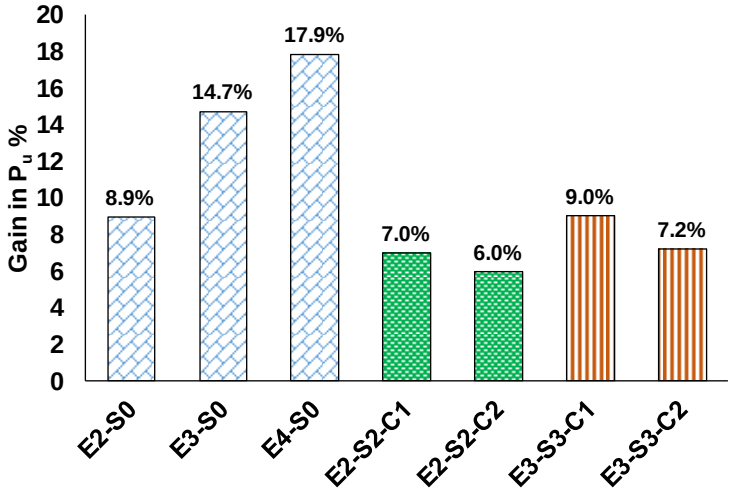

Figure 53: Gain in Pu % for EB strengthened specimens with and without steel stirrups.

By comparing the EB strengthened specimens with no steel stirrups at CSS, it was observed that the strengthened specimen with four EB-FRP experienced the highest load carrying capacity (264 kN), while that was 244 kN and 257 kN for the specimens with two and three EB-FRP, respectively. Correspondingly, the specimen (E4-S0) showed an increase in the load carrying capacity of 17.9%, while that ratio was 14.7% and 8.9% for the specimens E3-S0 and E2-S0, respectively as shown in Figure 54.

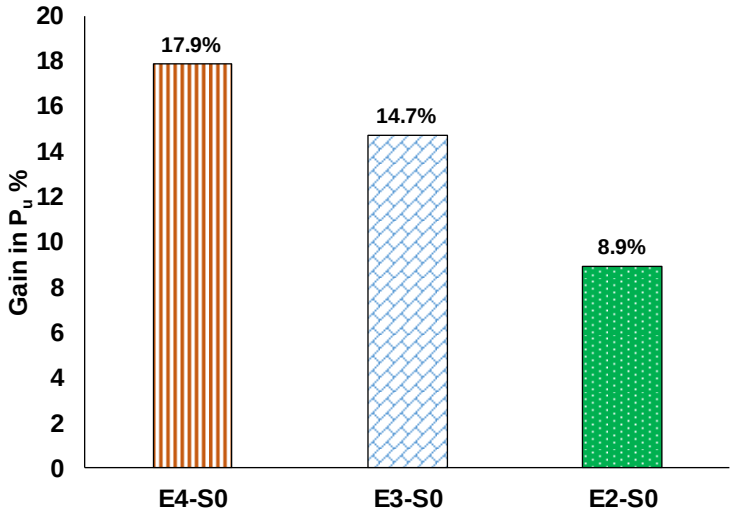

Figure 54: Gain in P_u % comparison in terms number of EB-FRP.

The ultimate load was affected by the relation between the steel stirrups and the EB-FRP at the CSS. Generally, specimens with aligned configuration showed a higher load carrying capacity than that for specimens with unaligned configuration. This observation indicates the effectiveness of placing the EB-FRP aligned to the steel stirrups at the CSS. However, this was the opposite of the NSM technique. For example, the beam with three EB-FRP and three steel stirrups aligned to each other (E3-S3-C1) has shown a load carrying capacity of 291 kN, while that was 282 kN for the beam with the same number of FRP and steel stirrups but unaligned to each other (E3-S3-C2).

The same trend was remarked for specimens with two EB-FRP. To illustrate, the beam with unaligned configuration (E2-S2-C2) exhibited an increase in the load carrying capacity of 6%, while that ratio was 7% for the beam with aligned configuration (E2-S2-C1). Figure 55 clearly illustrated this trend.

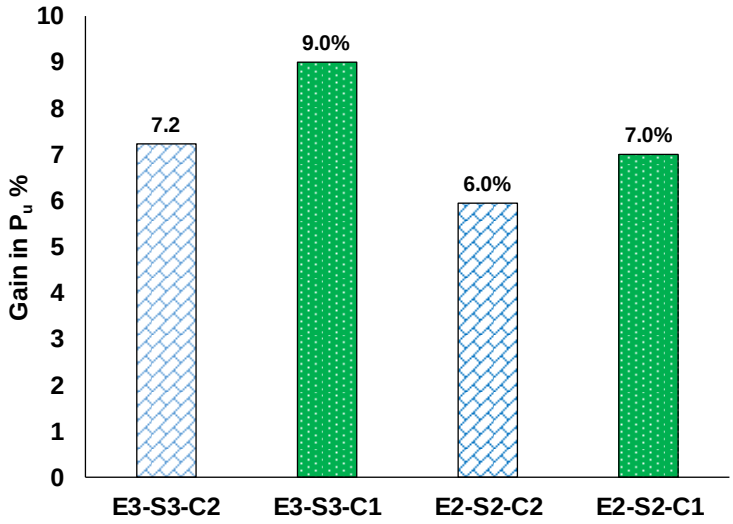

Figure 55: Gain in P_u % comparison between aligned and unaligned configurations.

4.3.2 Load-Deflection Response

The ultimate deflection that is corresponding to the ultimate load for EB strengthened specimens were listed in Table 5. Generally, it was remarked that the reference specimens experienced lower ultimate deflections than that for EB strengthened specimens. This proved the success of the EB technique to enhance the ductility behavior of the deep beams as well as the NSM technique. The increase in the deflection for the strengthened specimens has been listed in the third column of Table 6. The average ultimate deflection for reference beams was calculated to be 6.7 mm, while that was 8.5 mm for the EB strengthened beams, with difference percentage equal to 27.2%. This explained the effectiveness of the strengthening technique to enhance the ductility of the deep beams, which are known to have relatively brittle behavior.

Regards to the specimens without steel stirrups, the ultimate deflection was observed in the range from 8.5 mm to 9.1 mm with an average of 8.8 mm.

Correspondingly, the increase in the deflection has been reported in the range from 35.8% to 45.4% with an average of 40% for the specimens without steel stirrups. The lowest ultimate deflection was observed at specimen E2-S0 (δ =8.5 mm), while the

highest ultimate deflection was obtained at the strengthened beams with four EB-FRP (E4-S0, $\delta = 9.1$ mm). Using two EB-FRP increased the ultimate deflection by 35.8 %, while an increase in the ultimate deflection of 39% and 45.4% were achieved by using three and four EB-FRP, respectively.

The beams with three EB-FRP showed an increase in the ultimate deflection up to 39.6% compared to the corresponding reference specimen. However, an average increase in the ultimate deflection of 35.5% was obtained for all specimens with three EB-FRP. The beam with the aligned configuration between the steel stirrups and EB-FRP was found to have larger ultimate deflection than that for the specimen with unaligned configuration.

Approximately, the same behavior was noticed for all the specimens with two EB-FRP. Generally, the ultimate deflection on this set of beams ranged from 8.1 mm to 8.5 mm. The highest gain percentage on the ultimate deflection for specimens with two EB-FRP was 35.8% credited to the specimen without steel stirrups (E2-S0). However, the specimens with two EB-FRP and two steel stirrups E2-S2-C1 and E2-S2-C2 were able to show an increase in the ultimate deflection by 18.1% and 8.3%, respectively as shown in Figure 56. Specimens with aligned configuration were noticed to have relatively higher ultimate deflection than that for specimens with unaligned configuration. This behavior was the same in the NSM technique.

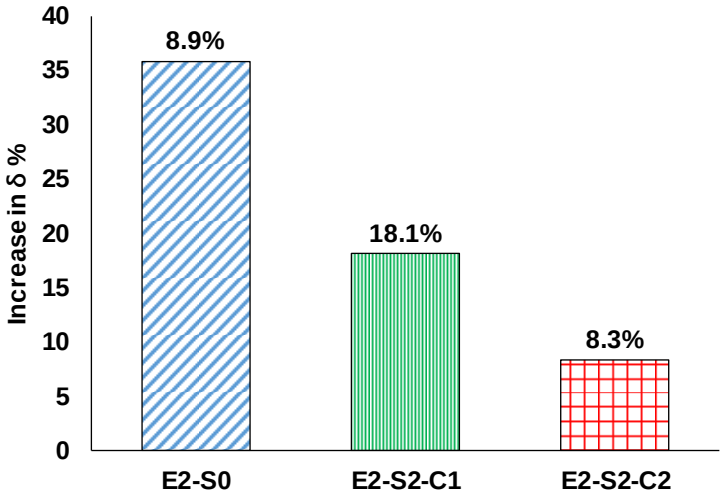

Figure 56: Increase in δ% for EB strengthened specimens with two EB-FRP.

The Figure 57a shows the load-deflection plots for specimens with no steel stirrups at the CSS, while Figure 57b and 57c present the load-deflection plots for specimens with two and three steel stirrups at the CSS, respectively. All specimens experienced a sudden drop in the load-displacement curve at the failure point. This was expected behavior due to the typical compression shear failure mode. Eventually, the ductility was found to be higher for the strengthened specimens with three EB-FRP than that for the specimens with two EB-FRP.

4.3.3 Energy Absorption

The energy absorption for each specimen has been listed in Table 5. Generally, it was observed that the EB strengthening technique increased energy absorption. The increase-percentage of the strengthened specimens was listed in the fourth column of Table 6.

For the EB strengthened specimens, the energy absorption ranged from 1069 kN.mm to 1330 kN.mm, with an average of 1213 kN.mm. This has corresponded to an average increase of 43.9% in the energy absorption for all EB strengthened specimens compared to the associated references.

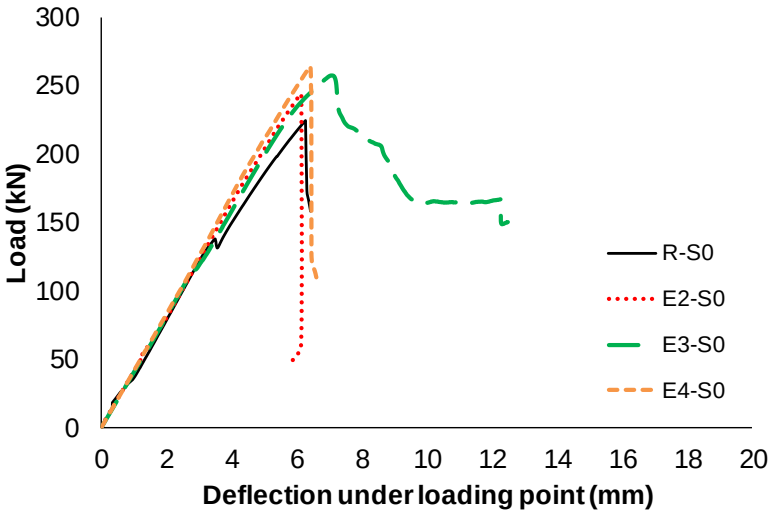

(a) Specimens with no steel stirrups at the CSS

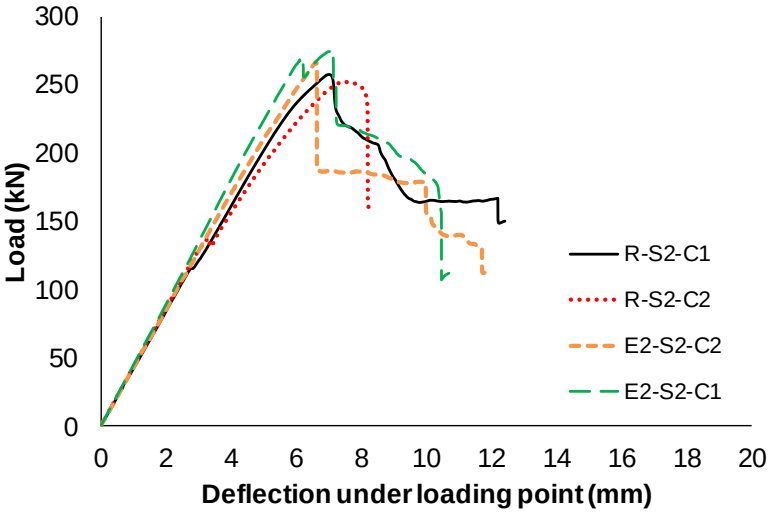

(b) Specimens with two steel stirrups at the CSS

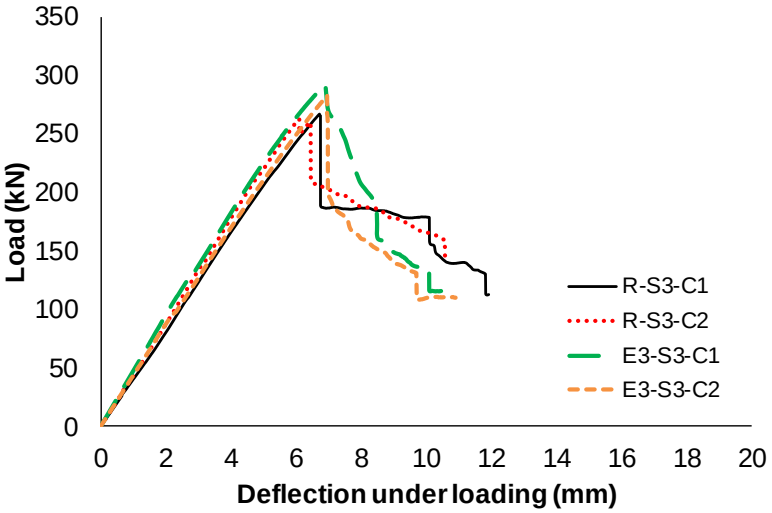

(c) Specimens with three steel stirrups at the CSS

Figure 57: Load-deflection plots for EB strengthened.

4.3.4 Strain Analysis

4.3.4.1. Tensile reinforcement strain

Similar to NSM specimens, four steel bars of 16 mm diameter were used in double layers as a typical tensile reinforcement. The flexural strain of the tensile reinforcements for the EB strengthened specimens has been listed in Table 5.

The flexural strain ranged from 2420 $\mu\varepsilon$ to 2843 $\mu\varepsilon$ with an average of 2746 $\mu\varepsilon$ for all EB strengthened specimens. Correspondingly, the average increase in the flexural strain was 11.9%. It was remarked that the specimens with aligned configuration have a lower increase in the flexural strain than that for specimens with unaligned configurations. This behavior was noticed for specimens with two and three EB-FRP.

The Figure 58a shows that the load-strain curves of the flexure reinforcement for specimens without steel stirrups at the CSS, while the Figure 58b and 58c show the load-strain curves for the flexure reinforcement for the specimens with two and three steel stirrups at the CSS, respectively. Generally, it can be noticed, that the more FRP used, the higher the ultimate stain was shown.

4.3.4.2. Stirrups strain

Total of four specimens was strengthened using EB technique with the presence of steel stirrups at the CSS. Overall, it has been reported that the strengthening technique significantly reduces the strain of the steel stirrups. The maximum strain of stirrups at the ultimate load for each specimen has been listed in Table 5. The average strain of stirrups for the reference specimens was observed 2679 $\mu\varepsilon$, while that was 1362 $\mu\varepsilon$ for the EB strengthened specimens. Specimens with unaligned configuration showed an average reduction of 56.8%, while that was 42.4% for specimens with aligned configuration.

4.3.4.3. Concrete strain

Similar to the NSM specimens, the strain of the concrete has been monitored during the test at each loading step using two strain gauges that were fixed on the concrete surface underneath the loading point. However, the strain gauges were damaged by the applied load during the test for two specimens: E3-S0 and E4-S0. Generally, there were no specimens exceeded the concrete crushing limit (3500 $\mu\varepsilon$). The average of the concrete strain for the reference beams was 1245 $\mu\varepsilon$, while that was 2485 $\mu\varepsilon$ for the EB strengthened beams. This has resulted in an average increase in the concrete strain of 56.4%. Furthermore, the number of EB-FRP used for strengthening was found to produce a considerable increase in the concrete compression strain. The average gain percentage of the concrete strain was reported to be 103.8% for beams with two EB-FRP and 96% for beams with three EB-FRP. The specimens with aligned configuration between the FRP and the shear stirrups were noticed to have lower concrete compression strain than that for the specimens with unaligned configuration. The average increase in the ultimate concrete strain was 85.3% for aligned configuration, while that was 131% for the specimens with unaligned configuration. Similar to the NSM specimens, the EB specimens with no shear stirrups in the CSS, were found to have the lowest increase in the ultimate concrete strain.

4.3.5 Failure Modes

All specimens failed in compression shear due to a major diagonal crack and debonding at the EB-FRP as shown in Figure 59a through 59g. The debonding was noticed to happen either between the epoxy and the concrete surface or between the EB-FRP and the epoxy, as shown in Figure 60a through 60e.

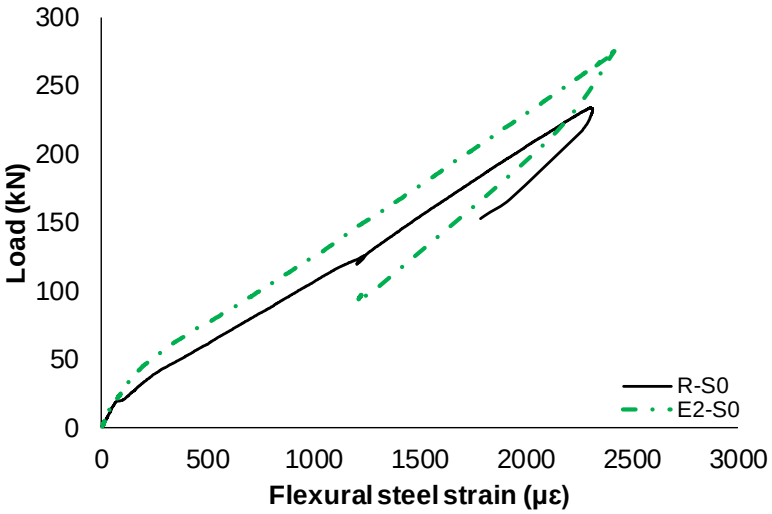

(a) Specimens with no steel stirrups at the CSS

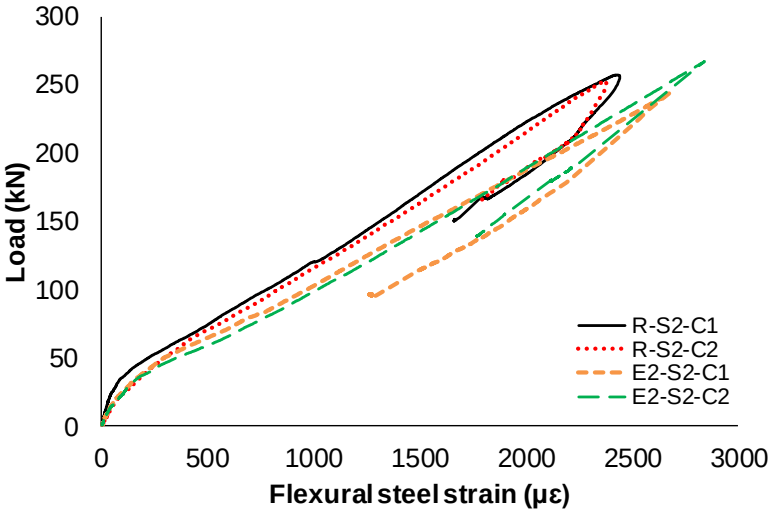

(b) Specimens with two steel stirrups at the CSS

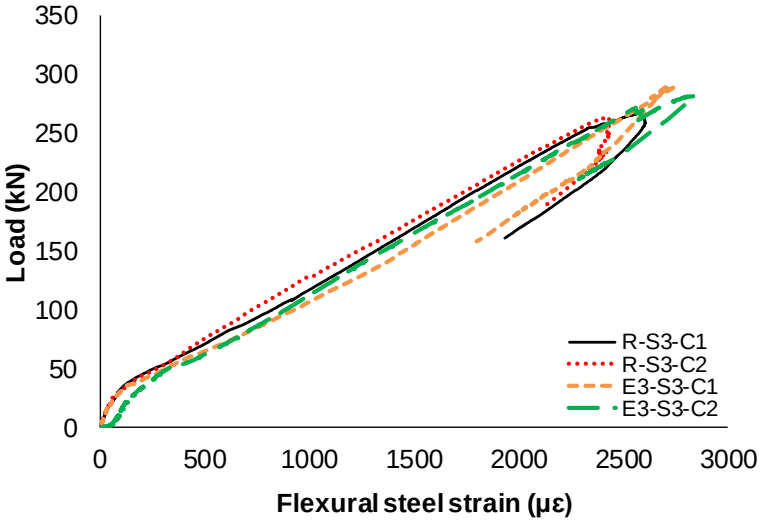

(c) Specimens with three steel stirrups at the CSS

Figure 58: Load-flexure steel strain plots for EB strengthened.

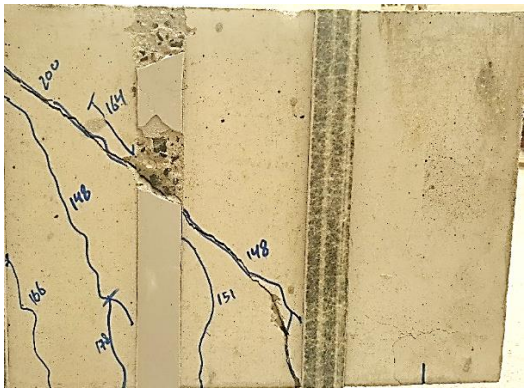

(a) E2-S0

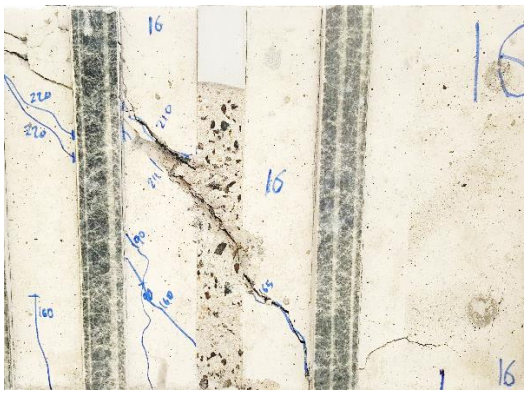

(b) E3-S0

(c) E4-S0

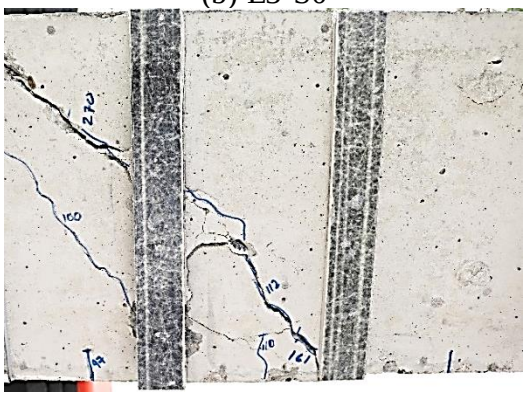

(d) E2-S2-C1

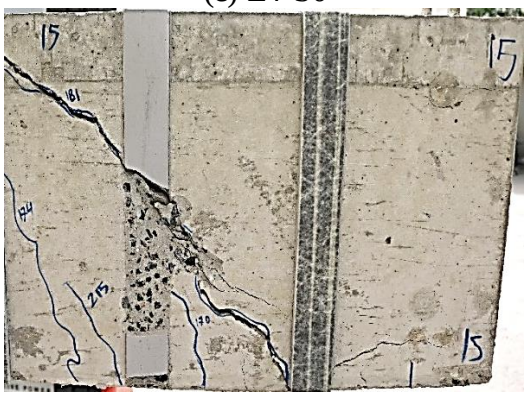

(e) E2-S2-C2

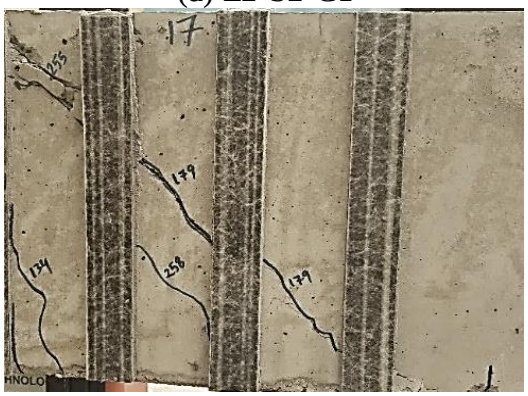

(f) E3-S3-C2

(g) E3-S3-C1

Figure 59: Crack pattern and failure mode for EB specimens (Front view).

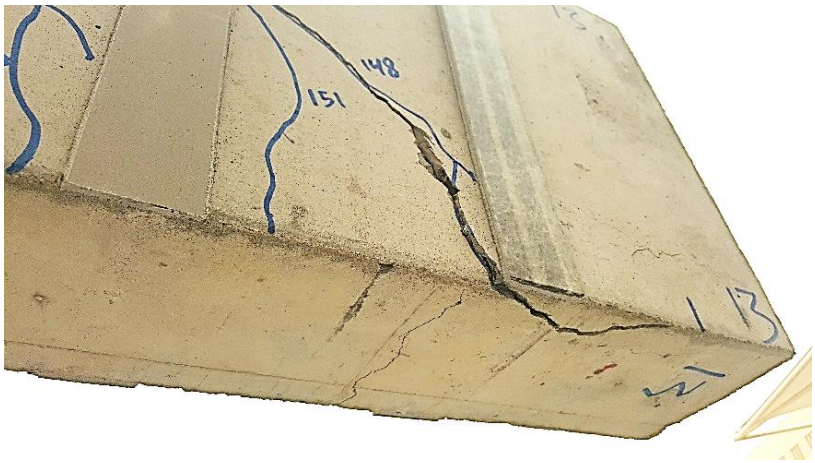

(a) E2-S0

(b) E3-S0

(c) E4-S0

(d) E3-S3-C1

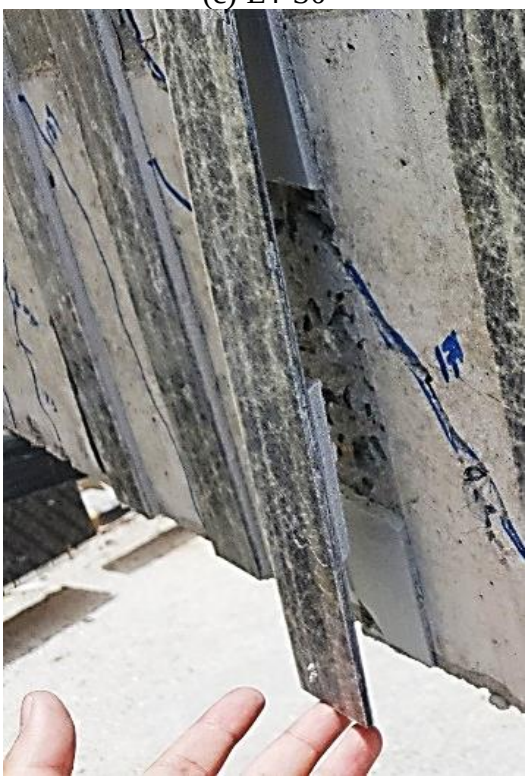

(e) E3-S3-C2

Figure 60: The debonding at the FRP for some EB specimens.

CHAPTER 5: THEORETICAL FORMULATION

This chapter provides a theoretical calculation to predict the ultimate load carrying capacity for the test specimens.

The nominal shear strength (V_n) for the strengthened beam is computed, as per ACI 318-05 [42], as follows:

$$V_n = V_c + V_s + \psi_f V_f \qquad (eq.1)$$

Where (V_c), (V_s), and (V_f) are the contributions of concrete, steel stirrups and the FRP strips at the critical shear span (CSS) to the total nominal shear strength, respectively. The reduction factor (ψ_f) $= 0.85$ as recommended for using the FRP from two opposite sides of the beam. Here, (V_c) is the experimental not the code-approximated value. The experimental value of the load carrying capacity for the reference specimen without steel stirrups, R-S0 is ($P_u = 224\ kN$). As the actual value of (V_c) is the reaction of the nearest support to the load (right-support), as shown in Figure 18; so,

$$V_c = \frac{P_u(L - L_{cr})}{L} \qquad (eq.2)$$

Where (L) is the total clear span between the two supports and (L_{cr}) is the critical shear span; substituting in equation 2,

$$V_c = \frac{224(1900 - 550)}{1900} = 159\ kN$$

The (V_s) is calculated using section 11.5.7.2 of the ACI318-05 [42] as follows:

$$V_s = A_{sv}\ f_{y_{sv}} \left(\frac{d}{s}\right) \qquad (eq.3)$$

Where the (A_{sv}) is the area of steel stirrups with yield stress ($f_{y_{sv}}$) that installed within spacing (s) at the critical shear span. A typical (A_{sv}) can be calculated for both sides, knowing that stirrups diameter is 6 mm, as follows:

$A_{sv} = 2\left(\frac{\pi d_{sv}^2}{4}\right) = 2\left(\frac{\pi(6)^2}{4}\right) = 56.6\ mm^2$ ($\times 2$ for the both sides of the steel stirrups)

Substituting in equation 3,

$V_s = 0$; for specimens without steel stirrups at the critical shear span

$V_s = 56.6 \times 234 \times \left(\frac{367}{200}\right) = 24.3\ kN$; for specimens with two stirrups $(s = 200\ mm)$

$V_s = 56.6 \times 234 \times \left(\frac{367}{135}\right) = 36.0\ kN$; for specimens with three stirrups $(s = 135\ mm)$

Then, the contribution of the FRP to the nominal shear strength V_f can be found as follows:

$$V_f = \frac{A_{f_v} f_{f_e} (\sin\alpha + \cos\alpha) d_{f_v}}{s_f} \qquad (eq.4)$$

Where the (A_{fv}) is the area of FRP to resist the shear, which can be found using the FRP strip's width $(w_f = 25\ mm)$ and thickness $(t_f = 3.18\ mm)$, as follows:

$A_{f_v} = 2nt_f w_f = 2(25 \times 3.18 \times 2) = 318\ mm^2$

The (d_{fv}) and (s_f) are referred to the effective depth of the FPR and the spacing between each groove, respectively. Since the FRP strips are applied vertically, $(\sin\alpha + \cos\alpha) = 1$. The total effective FRP stress (f_{f_e}) can be found from the Hook's low as follows:

$$f_{f_e} = \varepsilon_{f_e} E_f \qquad (eq.5)$$

But the effective strain of the FRP is determined as a fraction from the ultimate FRP strain using the factor (k_v) as follows:

$$\varepsilon_{f_e} = k_v \varepsilon_{f_u} \qquad (eq.6)$$

It is recommended to use the following formula to find the factor k_v:

$$k_v = \frac{k_1 k_2 L_e}{11900 \varepsilon_{f_u}} \leq 0.75 \qquad (eq.7)$$

Where (L_e) can be found as follows:

$$L_e = \frac{22300}{\left(2t_f E_f\right)^{0.58}} \qquad (eq.8)$$

Substituting in equation 8,

$$L_e = \frac{22300}{(2 \times 3.18 \times 6190)^{0.58}} = 13.2\ mm$$

Regards to the other factors k_1 and k_2, they can be found using the following formulas:

$$k_1 = \left(\frac{f_c'}{27}\right)^{\frac{2}{3}} \qquad (eq.9)$$

$$k_2 = \frac{d_{fv} - 2L_e}{d_v} \qquad (eq.10)$$

Substituting in equations 9 and 10,

$$k_1 = \left(\frac{40}{27}\right)^{\frac{2}{3}} = 1.3$$

$$k_2 = \frac{345 - 2(13.2)}{345} = 0.923$$

Eventually, from substituting in equation 7, the reduction factor k_v can be determined as follows:

$$k_v = \frac{(1.3)(0.923)(13.2)}{11900(0.013)} = 0.1$$

Now, the effective strain and its corresponding effective stress for the FRP can be calculated by substituting in equations 6 and 5 as follows:

$$\varepsilon_{f_e} = 0.1(0.013) = 0.0013 < 0.004$$

$$f_{f_e} = 0.0013(62190) = 80.8\ MPa$$

Finally, the FRP contribution to the nominal shear strength can be calculated for different configurations by substituting in equation 4 as follows:

For specimens with two NSM-FRP ($s_f = 200\ mm$):

$$V_f = \frac{318 \times 80.8 \times 1 \times 345}{200} = 44.3\ kN$$

For specimens with three NSM-FRP ($s_f = 135\ mm$):

$$V_f = \frac{318 \times 80.8 \times 1 \times 345}{135} = 65.7\ kN$$

For specimens with four NSM-FRP ($s_f = 100\ mm$):

$$V_f = \frac{318 \times 80.8 \times 1 \times 345}{100} = 88.6\ kN$$

Currently, the total nominal shear strength for each specimen can be calculated by taking the summation of its V_c , V_s and V_f by substituting in equation 1:

$$V_n = V_c + V_s + \psi_f V_f$$

The corresponding ultimate theoretical load can be calculated for each specimen as follows:

$$P_u^{th} = V_n \times \frac{L}{L - L_{cr}} \qquad (eq.12)$$

The ultimate theoretical load for each NSM strengthened specimen is listed in Table 7. By comparing the ultimate experimental load and the theoretical one, it was noticed that both are closed to each other with maximum difference of 12%. Figure 61 shows a comparison between the theoretical and experimental ultimate load for the NSM strengthened test specimens. However, the theoretical model was not representative for the EB strengthened specimens due to the FRP debonding, that was noticed at all the EB strengthened specimens. Therefore, more work is needed to determine the shear capacity of EB strengthened specimens taking into consideration the debonding behaviour. This may be a reduction factor or function of the fiber type and bond properties.

Table 7:

Theoretical & Experimental Ultimate Load for NSM Specimens

Specimen ID	P_u (kN)	P_u^{th} (kN)	P_u/P_u^{th}
R-S0	224	224	-
N2-S0	311	277	1.12
N3-S0	337	303	1.11
N4-S0	349	330	1.06
R-S2-C1	257	256	1.00
N2-S2-C1	331	309	1.07
R-S2-C2	252	256	0.98
N2-S2-C2	335	309	1.08
R-S3-C1	267	272	0.98
N3-S3-C1	369	351	1.05
R-S3-C2	263	272	0.97
N3-S3-C2	381	351	1.09

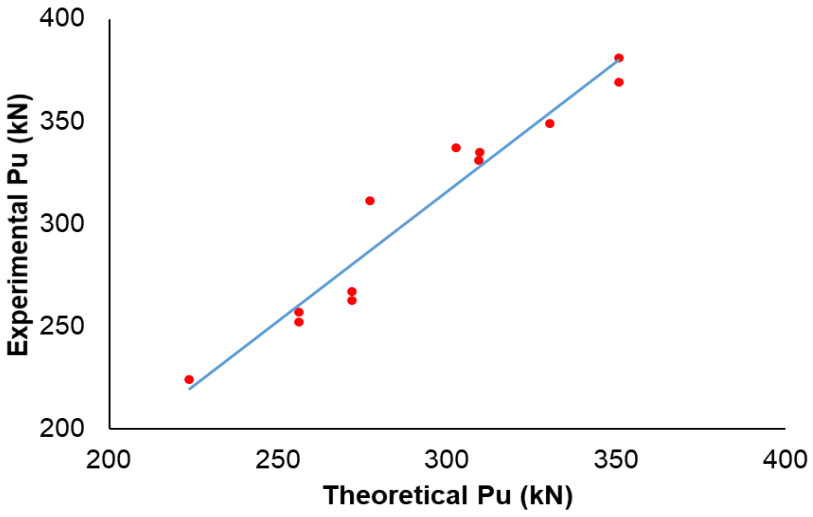

Figure 61: Theoretical versus experimental ultimate load for NSM specimens

CHAPTER 6: SUMMARY AND CONCLUSIONS

This thesis introduced an experimental study on the efficacy of using NSM-FRP and EB-FRP for the shear strengthening of RC rectangular deep beams. For this purpose, nineteen (19) shear deficient RC rectangular deep beams have been designed, fabricated, and tested. The interaction between the steel stirrups and FRP systems in the CSS has been investigated. The experimental results were intensively discussed in terms of the shear capacity, the deformation and ductility characteristics, the modes of failure, the crack propagation, and the strains. Different configurations for FRP and steel stirrups have been assessed. Test parameters for both NSM and EB techniques were: number of FRP (2, 3 and 4), number of steel stirrups at the CSS (0, 2 and 3), and the FRP/stirrups interaction at the CSS (aligned and unaligned). The main conclusions drawn from this study are summarized as follows:

- The theoretical model provides a good prediction to ultimate shear capacity for the NSM strengthened specimens but was not representative for the EB counterpart due to the FRP debonding behaviour.
- FRP can be used to significantly increase the load carrying capacity of shear deficient RC rectangular deep beams using both the NSM and EB strengthening techniques. However, the NSM technique exhibited better performance than that in the EB technique. An enhancement in the ultimate load carrying capacity ranging from 6% to 17.9% was observed using the EB system, while an increment from 28.8% to 55.8% was observed using the NSM counterpart. This enhancement is more than required in most of the practical strengthening application on the RC deep beams.

- Concerning the FRP configurations, it was observed that increasing the amount of the FRP, increases the load carrying capacity and strengthening gain percentage. This behavior was reported for both the NSM and EB technique. By comparing the specimens without steel stirrups at the CSS, NSM technique was able to enhance the load carrying capacity up to 55.8% while that was 17.9% using EB counterpart.
- The presence of the steel stirrups at the CSS was noticed to increase the load carrying capacity of the beam but decreases the efficacy of the FRP strengthening systems. An overall average of the gain in P_u% was found to be 31% for specimens without steel stirrups at the CSS, while that was 22% for specimens with steel stirrups at the CSS.
- Aligned configuration between steel stirrups and the FRP strengthening system was showed better performance in the EB technique, while the unaligned configuration was noticed to be better in the NSM technique. The average increase in the P_u% using EB technique was observed to be reduced from 8% at the aligned configuration to 6.6% at the unaligned configuration. In contrast, the average increase in P_u% using NSM technique was remarked to be increased from 33.5% at the aligned configuration to 38.9% at the unaligned configuration.
- Both EB and NSM strengthening techniques enhanced the deformational characteristics of specimens relative to their references. Overall, the ultimate deflection of the specimens has been increased by an average of 62.1% and 30.6% when using NSM and EB techniques, respectively.

- Moreover, the average gains in energy absorption were 173.2% and 43.9% relative to the references for the specimens strengthened using NSM and EB techniques, respectively.
- NSM strengthening technique has been remarked to significantly reduce the crack width at the ultimate load for the specimens. Overall, the average reduction in the ultimate crack width has been determined as 45% and 36% for specimens without and with steel stirrups at the CSS, respectively.
- Utilization of the FRP to enhance the shear capacity was reported to reduce the maximum strain in the steel stirrups at the CSS. The average maximum strain in the shear stirrups was reduced 39% using NSM technique and 51% using EB technique. This because the FRP strips resist some of the total applied stresses on the steel stirrups. In other words, both FRP and steel stirrups work together to reinforce the beam against the applied shear stresses.
- Both EB and NSM strengthening techniques were found to significantly increase the tensile strain in the flexure steel reinforcement and the compression strain in the concrete surface. Overall, an average increase in the tensile strain of the flexure reinforcement was found to be 70.4%, while that was 77.6% for the compression strain in the concrete surface.
- Unlike EB, the NSM technique improved the FRP/concrete bond; hence, increasing the utilization of the FRP strips at each groove. Generally, FRP debonding failure was significantly mitigated in the NSM, while was the governing failure mode in the EB. Most of the specimens failed in concrete compression shear failure. NSM strengthened specimens with three steel stirrups, and three NSM-FRP exhibited relatively more flexural bending before the rupture point.

REFERENCES

[1] Alba-Rodríguez MD, Martínez-Rocamora A, González-Vallejo P, Ferreira-Sánchez A, Marrero M. Building rehabilitation versus demolition and new construction: Economic and environmental assessment. Environ Impact Assess Rev 2017;66:115–26. doi:10.1016/j.eiar.2017.06.002.

[2] Badawi M, Soudki K. Flexural strengthening of RC beams with prestressed NSM CFRP rods - Experimental and analytical investigation. Constr Build Mater 2009;23:3292–300. doi:10.1016/j.conbuildmat.2009.03.005.

[3] Lorenzis L De, Nanni A. Proposed design procedure of NSM FRP reinforcement for strengthening of RC beams. Proceedings, 6th Int Symp Frp Reinf Concr Struct Singapore 2003:1455–1.

[4] Mostofinejad D, Tabatabaei Kashani A. Experimental study on effect of EBR and EBROG methods on debonding of FRP sheets used for shear strengthening of RC beams. Compos Part B Eng 2013;45:1704–13. doi:10.1016/j.compositesb.2012.09.081.

[5] Adhikary BB, Mutsuyoshi H. Shear strengthening of reinforced concrete beams using various techniques. Constr Build Mater 2006;20:366–73. doi:10.1016/j.conbuildmat.2005.01.024.

[6] Younis A, Ebead U, Shrestha KC. Different FRCM systems for shear-strengthening of reinforced concrete beams. Constr Build Mater 2017;153:514–26. doi:10.1016/j.conbuildmat.2017.07.132.

[7] Barnes RA, Baglin PS, Mays GC, Subedi NK. External steel plate systems for the shear strengthening of reinforced concrete beams. Eng Struct 2001;23:1162–76. doi:10.1016/S0141-0296(00)00124-3.

[8] Dizhur D, Griffith M, Ingham J. Improvement of unreinforced masonry wall panels shear strength using NSM CFRP strips. Int Mason Conf 2014 2013;17:1–13. doi:10.1061/(ASCE)CC.1943-5614.0000400.

[9] Ebead U, Saeed H. Modeling of inexpensive strengthening technique for reinforced concrete beams. ACI Struct J 2017;114:451–62. doi:10.14359/51689444.

[10] Ebead U. Inexpensive Strengthening Technique for Partially Loaded Reinforced Concrete Beams : Experimental Study. J Mater Civ Eng 2015;27:1–11. doi:10.1061/(ASCE)MT.1943-5533.0001249.

[11] Ebead UA, Wakjira TG. Behaviour of RC beams strengthened in shear using near surface embedded FRCM. CONCET 2018 - 14th Int. Conf. Concr. Eng. Technol., 2018.

[12] D'Ambrisi A, Feo L, Focacci F. Bond-slip relations for PBO-FRCM materials externally bonded to concrete. Compos Part B Eng 2012;43:2938–49. doi:10.1016/j.compositesb.2012.06.002.

[13] Wakjira TG, Ebead U. Hybrid NSE/EB technique for shear strengthening of reinforced concrete beams using FRCM: Experimental study. Constr Build Mater 2018;164:164–77. doi:10.1016/j.conbuildmat.2017.12.224.

[14] Pino V, Akbari Hadad H, De Caso y Basalo F, Nanni A, Ali Ebead U, El Refai A. Performance of FRCM-Strengthened RC Beams Subject to Fatigue. J Bridg Eng 2017;22:04017079. doi:10.1061/(ASCE)BE.1943-5592.0001107.

[15] Younis A, Ebead U. Characterization and application of FRCM as a strengthening material for shear-critical RC beams. 5th Int. Conf. Concr. Repair,

Rehabil. Retrofit. ICCRRR 2018, 2018.

[16] Younis A, Ebead U, Shrestha KC. FRCM Shear Strengthening for Concrete Beams. Proc. Ninth Int. Struct. Eng. Constr. Conf. Resilient Struct. Sustain. Constr., 2017.

[17] Rizzo A, De Lorenzis L. Behavior and capacity of RC beams strengthened in shear with NSM FRP reinforcement. Constr Build Mater 2009;23:1555–67. doi:10.1016/j.conbuildmat.2007.08.014.

[18] Guadagnini M, Pilakoutas K, Waldron P. Shear Resistance of FRP RC Beams: Experimental Study. J Compos Constr 2006;10:464–73. doi:10.1061/(ASCE)1090-0268(2006)10:6(464).

[19] Chen GM, Chen JF, Teng JG. On the finite element modelling of RC beams shear-strengthened with FRP. Constr Build Mater 2012;32:13–26. doi:10.1016/j.conbuildmat.2010.11.101.

[20] Baky HA, Ebead U a., Neale KW. Flexural and Interfacial Behavior of FRP-Strengthened Reinforced Concrete Beams. J Compos Constr 2007;11:629–39. doi:10.1061/(ASCE)1090-0268(2007)11:6(629).

[21] Kim G, Sim J, Oh H. Shear strength of strengthened RC beams with FRPs in shear. Constr Build Mater 2008;22:1261–70. doi:10.1016/j.conbuildmat.2007.01.021.

[22] Ebead U, Saeed H. FRP/stirrups interaction of shear-strengthened beams. Mater Struct Constr 2017;50:1–16. doi:10.1617/s11527-016-0973-7.

[23] Fukuyama K, Higashibata Y, Miyauchi Y. Studies on repair and strengthening methods of damaged reinforced concrete columns. Cem Concr Compos

2000;22:81–8. doi:10.1016/S0958-9465(99)00044-X.

[24] Pham TM, Doan L V., Hadi MNS. Strengthening square reinforced concrete columns by circularisation and FRP confinement. Constr Build Mater 2013;49:490–9. doi:10.1016/j.conbuildmat.2013.08.082.

[25] Parvin A, Brighton D. FRP composites strengthening of concrete columns under various loading conditions. Polymers (Basel) 2014;6:1040–56. doi:10.3390/polym6041040.

[26] Elsayed WE, Ebead UA, Neale KW. Analysis of FRP-strengthened Two-way Slabs. Polymer (Guildf)., 2006.

[27] Ebead U, Marzouk H. Fiber-reinforced polymer strengthening of two-way slabs. ACI Struct J 2004;101:650–9. doi:10.14359/13387.

[28] Elsayed WE, Ebead UA, Neale KW. Investigations on mechanically fastened FRP-strengthened concrete slabs. FFourth Int Conf FRP Compos Civ Eng 2008:1–6.

[29] Ebead U, Marzouk H. Strengthening of two-way slabs subjected to moment and cyclic loading. ACI Struct J 2002;99:435–44.

[30] Elsayed WE, Ebead UA, Neale KW. Mechanically Fastened FRP-Strengthened Two-Way Concrete Slabs with and without Cutouts. J Compos Constr 2009;13:198–207. doi:10.1061/(ASCE)CC.1943-5614.0000004.

[31] Elsayed W, Ebead UA, Neale KW, Asce M. in FRP-Strengthened Concrete Slabs 2007;11:619–28.

[32] Baky HA, Ebead UA, Neale KW. Statistical Analyses and Parametric Study for Flexure with FRPs 2010;13:805–22.

[33] Kotynia R, Abdel Baky H, Neale KW, Ebead UA. Flexural strengthening of RC beams with externally bonded CFRP systems: Test results and 3D nonlinear FE analysis. J Compos Constr 2008;12:190–201. doi:Doi 10.1061/(Asce)1090-0268(2008)12:2(190).

[34] Täljsten B, Elfgren L. Strengthening concrete beams for shear using CFRP-materials : evaluation of different application methods 2000;31:87–96.

[35] Nanni A, Lorenzis L De, Nanni A. Shear Strengthening of Reinforced Concrete Beams with Near-Surface Mounted Fiber-Reinforced Polymer Rods. ACI Struct J 2001;98.

[36] Khalifa A, Nanni A. Rehabilitation of rectangular supported RC beams with deficiencies using CFRP composites. Constr Build Mater 2002;16:135–46.

[37] Tang CY, Tan KH, Asce A, Tan KH, Asce M. Interactive Mechanical Model for Shear Strength of Deep Beams. J Struct Eng 2004;130:1534–44. doi:10.1061/(ASCE)0733-9445(2004)130:10(1534).

[38] Elmezaini N. Demolition or Restoration: A Case Study. Br J Appl Sci Technol 2015;10:1–10. doi:10.9734/bjast/2015/19513.

[39] Costa AG, Guedes J, Varum H. Structural Rehabilitation of Old Buildings. vol. 2. 2014. doi:10.1007/978-3-642-39686-1.

[40] Minafò G. A practical approach for the strength evaluation of RC columns reinforced with RC jackets. Eng Struct 2015;85:162–9. doi:10.1016/j.engstruct.2014.12.025.

[41] Jacketing Concrete Column n.d.

[42] Alkhrdaji T, Thomas J. Structural Strengthening Using External Post-Tensioning

Systems. Struct Mag 2009:8–10.

[43] Structral Technology. External/Internal Post Tensioning Systems n.d.

[44] Alkhrdaji T. Design and Application Techniques Key to Successful Structural Strengthening Projects n.d.

[45] Lorenzis L De, Teng JG. Near-surface mounted FRP reinforcement : An emerging technique for strengthening structures. Compos Part B 2007;38:119–43. doi:10.1016/j.compositesb.2006.08.003.

[46] Barros JAO, Dias SJE. Near surface mounted CFRP laminates for shear strengthening of concrete beams. Cem Concr Compos 2006;28:276–92. doi:10.1016/j.cemconcomp.2005.11.003.

[47] Costa IG, Barros JAO. Flexural and shear strengthening of RC beams with composite materials - The influence of cutting steel stirrups to install CFRP strips. Cem Concr Compos 2010;32:544–53. doi:10.1016/j.cemconcomp.2010.03.003.

[48] Bilotta A, Ceroni F, Di Ludovico M, Nigro E, Pecce M, Manfredi G. Bond Efficiency of EBR and NSM FRP Systems for Strengthening Concrete Members. J Compos Constr 2011;15:757–72. doi:10.1061/(ASCE)CC.1943-5614.0000204.

[49] Hassan T, Rizkalla S. Investigation of bond in concrete structures strengthened with near surface mounted carbon fiber reinforced polymer strips. J Compos Constr 2003;7:248–57. doi:10.1061/(ASCE)1090-0268(2003)7:3(248).

[50] ACI 318. Building Code Requirements for Structural Concrete. vol. 2007. 2011. doi:10.1016/0262-5075(85)90032-6.

[51] El Maaddawy T, Sherif S. FRP composites for shear strengthening of reinforced concrete deep beams with openings. Compos Struct 2009;89:60–9. doi:10.1016/j.compstruct.2008.06.022.

[52] Tan KH, Cheng GH. Size Effect on Shear Strength of Deep Beams: Investigating with Strut-and-Tie Model. J Struct Eng 2006;132:673–85. doi:10.1061/(ASCE)0733-9445(2006)132:5(673).

[53] Raj LJ, Rao AG. Shear Strength of Rc Deep Beam Panels – a Review. Int J Res Eng Technol 2014;03:2321–7308. doi:10.15623/ijret.2014.0328015.

[54] Anwarul Islam AKM. Effective methods of using CFRP bars in shear strengthening of concrete girders. Eng Struct 2009;31:709–14. doi:10.1016/j.engstruct.2008.11.016.

[55] Dias SJE, Barros JAO. Experimental behaviour of RC beams shear strengthened with NSM CFRP laminates. Strain 2012;48:88–100. doi:10.1111/j.1475-1305.2010.00801.x.

[56] Al-Mahmoud F, Castel A, Minh TQ, François R. Reinforced Concrete Beams Strengthened with NSM CFRP Rods in Shear. Adv Struct Eng 2015;18:1563–74. doi:10.1260/1369-4332.18.10.1563.

[57] Lorenzis L De, Nanni A. Shear Strengthening of Reinforced Concrete Beams with Near-Surface Mounted Fiber-Reinforced Polymer Rods 2001.

[58] Rahal KN, Rumaih HA. Tests on reinforced concrete beams strengthened in shear using near surface mounted CFRP and steel bars. Eng Struct 2011;33:53–62. doi:10.1016/j.engstruct.2010.09.017.

[59] Chaallal O, Mofidi A, Benmokrane B, Neale K. Embedded Through-Section

FRP Rod Method for Shear Strengthening of RC Beams: Performance and Comparison with Existing Techniques. J Compos Constr 2011;15:374–83. doi:10.1061/(ASCE)CC.1943-5614.0000174.

[60] Grande E, Imbimbo M, Rasuolo A. Effect of transverse steel on the response of RC beams strengthened in shear by FRP: Experimental study. J Compos Constr 2009;13:405–14. doi:10.1061/(ASCE)1090-0268(2009)13:5(405).

[61] Islam MR, Mansur MA, Maalej M. Shear strengthening of RC deep beams using externally bonded FRP systems. Cem Concr Compos 2005;27:413–20. doi:10.1016/j.cemconcomp.2004.04.002.

[62] Zhang Z, Hsu C-TT, Moren J. Shear Strengthening of Reinforced Concrete Beams Using Carbon Fiber Reinforced Polymer Laminate: A Review. J Compos Constr 2004;8:403–14. doi:10.1061/(ASCE)1090-0268(2004)8:5(403).

[63] Almassri B, Al Mahmoud F, Francois R. Behaviour of corroded reinforced concrete beams repaired with NSM CFRP rods, experimental and finite element study. Compos Part B Eng 2016;92:477–88. doi:10.1016/j.compositesb.2015.01.022.

[64] Lee HK, Cheong SH, Ha SK, Lee CG. Behavior and performance of RC T-section deep beams externally strengthened in shear with CFRP sheets. Compos Struct 2011;93:911–22. doi:10.1016/j.compstruct.2010.07.002.

[65] Bousselham A, Chaallal O. Effect of transverse steel and shear span on the performance of RC beams strengthened in shear with CFRP. Compos Part B Eng 2006;37:37–46. doi:10.1016/j.compositesb.2005.05.012.

[66] Li W, Leung CKY. Shear Span–Depth Ratio Effect on Behavior of RC Beam

Shear Strengthened with Full-Wrapping FRP Strip. J Compos Constr 2016;20. doi:10.1061/(ASCE)CC.1943-5614.0000627.

[67] Barros J, Dias S. Assessment of the effectiveness of the NSM shear strengthening technique for deep T cross section RC beams 2013:1–10.

[68] Dias SJE, Barros JAO. Shear strengthening of RC T-section beams with low strength concrete using NSM CFRP laminates. Cem Concr Compos 2011;33:334–45. doi:10.1016/j.cemconcomp.2010.10.002.

[69] Barros JAO, Dias SJE, Lima JLT. Efficacy of CFRP-based techniques for the flexural and shear strengthening of concrete beams. Cem Concr Compos 2007;29:203–17. doi:10.1016/j.cemconcomp.2006.09.001.

[70] ASTM C1314. Standard Test Method for Compressive Strength of Masonry Prisms. ASTM Int 2015:1–10. doi:10.1520/C0039.

[71] C496. Splitting Tensile Strength of Cylindrical Concrete Specimens. ASTM Stand 2014;i:1–5. doi:10.1520/C0496.

[72] ASTM A370. Standard test methods and definitions for mechanical testing of steel products. ASTM Stand 2014:1–50. doi:10.1520/A0370-14.2.

[73] SAFSTRIP. SAFSTRIP ® FIBER REINFORCED STRENGTHENING STRIP Materials of Construction n.d.

[74] Sheet PD. Sikadur ® -30 LP THIXOTROPIC ADHESIVE FOR BONDING REINFORCEMENT 2017:2–5.

[75] HILTI DC-SE20 Slitting Machine. DC-SE 20 n.d. https://www.hilti.com.qa/c/CLS_POWER_TOOLS_7124/CLS_DIAMOND_CUTTING_SLITTING_TOOLS_7124/CLS_SLITTING_TOOLS_7124/r1740.

[76] Ombres L. Structural performances of reinforced concrete beams strengthened in shear with a cement based fiber composite material. Compos Struct 2015;122:316–29.

[77] Ebead U, Shrestha KC, Afzal MS, El Refai A, Nanni A. Effectiveness of Fabric-Reinforced Cementitious Matrix in Strengthening Reinforced Concrete Beams. J Compos Constr 2017;21:04016084. doi:10.1061/(ASCE)CC.1943-5614.0000741.